



**HAL**  
open science

## Characterization of micro-ZnO/PDMS composite structured via dielectrophoresis – Toward medical application

Xiaoting Zhang, Minh-Quyen Le, Van-Cuong Nguyen, Jean-François Mogniotte, Jean-Fabien Capsal, Daniel Grinberg, Pierre-Jean Cottinet, Lionel Petit

### ► To cite this version:

Xiaoting Zhang, Minh-Quyen Le, Van-Cuong Nguyen, Jean-François Mogniotte, Jean-Fabien Capsal, et al.. Characterization of micro-ZnO/PDMS composite structured via dielectrophoresis – Toward medical application. *Materials & Design*, 2021, 208, pp.109912. 10.1016/j.matdes.2021.109912 . hal-03662184

**HAL Id: hal-03662184**

**<https://hal.science/hal-03662184>**

Submitted on 2 Aug 2023

**HAL** is a multi-disciplinary open access archive for the deposit and dissemination of scientific research documents, whether they are published or not. The documents may come from teaching and research institutions in France or abroad, or from public or private research centers.

L'archive ouverte pluridisciplinaire **HAL**, est destinée au dépôt et à la diffusion de documents scientifiques de niveau recherche, publiés ou non, émanant des établissements d'enseignement et de recherche français ou étrangers, des laboratoires publics ou privés.



Distributed under a Creative Commons Attribution - NonCommercial 4.0 International License

# Characterization of micro-ZnO/PDMS Composite Structured via Dielectrophoresis – Toward medical application

Xiaoting Zhang<sup>1</sup>, Minh-Quyen Le<sup>1\*</sup>, Van-Cuong Nguyen<sup>1</sup>, Jean-François Mognotte<sup>1,2</sup>, Jean-Fabien Capsal<sup>1</sup>, Daniel Grinberg<sup>3</sup>, Pierre-Jean Cottinet<sup>1</sup>, Lionel Petit<sup>1</sup>.

<sup>1</sup> Univ Lyon, INSA-Lyon, LGEF, EA682, F-69621, Villeurbanne, France

<sup>2</sup> HYBRIA Institute of Business and Technologies, Écully Campus, 69130 Écully, France

<sup>3</sup> Department of Cardiac Surgery, “Louis Pradel” Cardiologic Hospital, Lyon, France

\* Corresponding author: [minh-quyen.le@insa-lyon.fr](mailto:minh-quyen.le@insa-lyon.fr)

**Abstract:** This paper proposed a new approach to achieve full characteristic of highly non-linear current density-electric field (J-E) curve, which depends on various key factors in terms of filler concentration, temperature, input voltage level, and structuration of ZnO particles (i.e. aligned or randomly dispersed). The homogeneity of particle distribution within the polymer matrix, together with the chain-like structure of the aligned composites elaborated with various ZnO volume fraction was verified via microscopic investigations. Numerical simulation was also conducted through COMSOL Multiphysics, giving an estimation of field distribution around ZnO phase. Experimental characterization in addition to analytical models was established using varying (sinusoidal) or direct current (DC) tests. The DC test was carried out in order to identify the conduction profile as well as the percolation threshold of ZnO samples. Temperature also has considerable influence on the switching field and the dielectric permittivity of the nonlinear composites. In the sinusoidal test, current discrimination was adopted using bipolar polarization loop, allowed the detailed quantification of conductivity values, while prediction in the capacitive current density enabled to distinguish the relative permittivity. These results demonstrated that the electrical properties of ZnO compound, such as conductivity and permittivity, substantially enhanced with the increasing filler content, especially when the samples were subjected to dielectrophoretic manipulation. Further analysis was carried out on sinusoidal unipolar polarization to predict the dielectric loss factor as function applied field. Finally, by playing on different pertinent parameters, it was possible to efficiently control the electric and mechanical characteristics of ZnO composite. Such properties are highly important in application of microvaristors used as protection devices. By associating with other features of ZnO like piezoelectricity, this material is undoubtedly of high interest in medical use where multifunctional system design becomes mandatory.

**Keywords:** Micro ZnO composites, Structured materials, Dielectrophoresis method, Electric and mechanical characterizations, Dielectric and conduction losses, Temperature stability.

## 1. Introduction

Zinc oxide (ZnO)-based composite material, where ZnO particles are embedded in the polymer, attracts increasing interests due to the combination of the remarkable intrinsic properties of ZnO and the mechanical flexibility, stability of polymer matrix [1–6]. Owing to the excellent electric, optical, piezoelectric properties of ZnO, ZnO composites are utilized in a wide application such as microvaristors, thin film transistors, biosensor, energy harvester [7–10]. As compared to traditional piezoelectric transducer like piezo-ceramic lead zirconate titanate (PZT) [11,12] and poly(vinylidene fluoride) piezopolymers [13], ZnO/polymer composite is regarded as potential candidate for commercial piezoelectric thin film due to the low-cost fabrication, abundance, biocompatible and mechanical properties. It has been

demonstrated that when blending ZnO nanoparticles into a photosensitive polymer matrix (SU-8), a comparable piezoelectric coefficient, up to  $23 \text{ pmV}^{-1}$ , was observed [14].

Microvaristor is one of important applications using composite based polymeric matrix filled with semi-conductor (e.g. ZnO) powder [15]. Such a device is widely used to minimize the localized field enhancement, making microvaristor compounds great potential to vary and adapt electrical characteristics. For conventional varistors, a high sintering temperature (around  $1000 \text{ }^\circ\text{C}$ ) is required to form stereotyped pattern, meanwhile ZnO-based microvaristor composites only need a curing temperature of around  $100 \text{ }^\circ\text{C}$  and enable to construct into the flexible substrates, shapes. Therefore, ZnO microvaristors are widely employed in the high voltage application such as stator coils, polymer insulator, electric-field grading of bushing, cable accessories [16–19]. Recently, the electric nonlinear field-dependent conductivity has been characterized in ZnO-epoxy, ZnO-LLDPE, ZnO-LDPE when the filler concentration above the percolation threshold [20–22]. A fundamental knowledge of the ZnO microvaristor is necessary to understand its non-linear characteristics, which is considered as dependent on the particle concentration, material properties, and voltage application.

In previous work, the effects of ZnO filler concentration on the electric, dielectric and piezoelectric properties of ZnO/PDMS thin film have been confirmed [24]. One of the key factors that influences these properties is the arrangement of the phases such as chain-like structure. Indeed, the connectivity of the filler controls the distribution of the electric flow in the material [25,26]. Composites with 0-3 connectivity, which consists of homogeneously dispersed particles in the matrix, are the most commonly produced because of their simple fabrication [26,27]. However, they require large volumetric contents to achieve reasonable performance, which considerably deteriorates the mechanical properties. A solution to this problem is to align the fillers in columns within the matrix. In anisotropic structure, called 1-3, the particles are closely aligned in preferred direction, allowing to boost the electromechanical coupling of the composite without increasing too much its concentration [13]. It was demonstrated in [24] that significant enhancement in the dielectric and piezoelectric behavior has been achieved through dielectrophoretic manipulation of ZnO particles, as opposed to the 0-3 matrix.

With the aim of efficiently exploiting potential of ZnO based PDMS polymer in microvaristor application, more detailed analysis of their electrical and mechanical properties is involved in this study. Actually, previous work [24] only dealt with the dielectric and piezoelectric of ZnO materials under low electric field. It should be understood that when the applied input exceeds the switching field, ZnO becomes more conductor than capacitor, which is manifested by its semiconductor properties. To fully assess the dielectric and piezoelectric performances of ZnO composite, it is important to thoroughly analyze the electric response under a high voltage excitation as well. To some extents, the resulting current of ZnO sample can be modeled by three components including ferroelectric, dielectric, and conduction mechanisms. The weighting given to each component strongly depends on the material properties and essentially on the applied voltage level. Consequently, exploring behavior of polarization hysteresis loop of ZnO microvaristor under large range of electric field becomes mandatory to further understand its nonlinear characteristics. Few research works have clearly identified these three mechanisms of ZnO materials. Eventually, the field effect of dielectric losses was not addressed either, despite its important contribution under low frequency and high input voltage.

Experimental characterizations together with theoretical model developed in this work are of interest to efficiently exploit ability of ZnO composite, which is revealed to be promising in piezoelectric and/or semiconductor devices. Previous work [24] showed a potential of ZnO composite as piezoelectric sensor for measuring pressure in heart or blood vessels, thanks to its biocompatibility. Always in medical field, this work, however, presented another application of ZnO based on its semi-conductor behavior. The objective consists of developing of a smart catheter used in PFA (pulse field ablation) to treat cardiac arrhythmias. On one hand, ZnO can be used to efficiently drive the electric field into the heart tissue, thanks to its good dielectric property. On the other hand, it can be exploited as microvaristor due to its

nonlinear electrical behavior. The system allows to trigger corona and partial discharges in high voltage equipment during PFA procedure, ensuring patient's safety [28].

The principal task of this study is to perform a full characterization of ZnO/PDMS composite involving electric and mechanical properties, as well the influence of dielectrophoretic orientation together with filler concentration. The structure of the paper is organized as follows. Firstly, section 2 discusses the film fabrication process as well as characterization methods to get the electrical and mechanical responses. Tests for temperature stability of 0-3 and 1-3 composites are also described. Secondly, results and comments are carried out in section 3 including several objectives that are outlined below:

- Microscopic evaluations are conducted to examine the alignment effect of material doped with various filler concentration.
- Electric field distribution of 0-3 and 1-3 ZnO/PDMS matrix has been modelled and simulated in COMSOL model.
- Current density vs. field (J-E) characteristics under DC test are performed in order to identify the switching field (i.e. relating to the percolation threshold of conducting path) and the conductivity of all samples, either random or aligned structure. Temperature stability are also investigated in both dielectric spectroscopy and electrical test.
- J-E characteristics under unipolar and bipolar high voltage applications are carried out. Analytical models together with experiment are involved to identify different components (i.e., ferroelectric polarization, capacitive behavior, and conduction mechanism-based Ohm and hopping effect) contributing to the current response. Relevant parameters such as permittivity, conductivity, and dielectric losses were extracted from the J-E curve.
- Mechanical characteristics-based stress-strain curve is performed, making a simple way to estimate the Young modulus as well as the ultimate tensile strength of all developed composites.

Thirdly, section 4 shows a potential application of the developed material in medical field, especially for the recent technique of PFA. Finally, concluding remarks and future perspective are drawn in section 5.

## **2. Fabrication of composites and method of characterization**

### *2.1. ZnO/PDMS composites film fabrication*

ZnO micropowder (~10  $\mu\text{m}$ , 99.9% purity) were provided by US Research Nanomaterials Inc. with a mass density of 5.6  $\text{g}/\text{cm}^3$ . The polydimethylsiloxane (PDMS) elastomer kit including base and curing agent were purchased from Trademark of The Dow Chemical Company. In order to analyze the impact of ZnO content on the properties of composite, four different volume fractions of ZnO (consisting of 10%, 20% 30%, 40%) were prepared. Among them, 0-3 composite films doped with ZnO particles randomly dispersed were fabricated through solution casting method. Meanwhile, 1-3 composite films with aligned ZnO particles were elaborated via dielectrophoretic manipulation. This method employed a high electric field of 1  $\text{V}/\mu\text{m}$  amplitude and 1 Hz frequency subjecting to the sample during the curing process. The detail fabrication has been elaborated in previous work [24]. The thickness of the samples, which is difficult to be controlled during the dielectrophoresis, are quite different (i.e. around 500-700  $\mu\text{m}$ ). The thickness of samples was precisely measured using a mechanical comparator (Florenza) to calculate the stress.

### *2.2. Electrical characterization*

Circular gold electrodes with a 20mm diameter and 30nm thick were deposited on both sides of samples by sputter coater (Cressington, 208HR). A film of 25 mm diameter was clamped in a sample holder between two copper electrodes. Firstly, a high voltage (DC or sinusoidal) was applied on the electrode of the film using a waveform generator (Agilent, 33210A) coupled with a high voltage amplifier (Trek, Model 20/20C). Secondly, the resulting was detected by a low-noise current preamplifier (Stanford

Research Systems, SR570) with a gain setting from 10-500  $\mu\text{A/V}$ . Lastly, these signals were monitored and recorded in digital storage oscilloscope (KEYSIGHT, DSOX1102G). It is noteworthy that an application of sinusoidal waveform allows to achieve polarization loop of all samples. Analytical model was then carried out so as to distinguish the conduction, the dielectric, and the ferroelectric responses. On the other hand, under DC electric field application, only conduction behavior got involved, making it possible to accurately determine the electric conductivity.

Broadband dielectric spectroscopy of the composites was performed using an impedance-analyzer (Solartron SI-1255 together with an interface 1296) at ambient temperature via a sample holder (AMETEK, 12962A). The dielectric spectra were acquired using a varying electric field with an amplitude of 1  $\text{V}_{\text{rms}}$  and a frequency range of 0.1 Hz to 1 MHz.

### 2.3. Temperature stability

In order to investigate the influence of temperature on the electric polarization loop, the entire sample holder was placed into an oven (Votsch Industrietechnik<sup>TM</sup>, VT7004), allowed the control of temperature with high precision. Samples were exposed to a large temperature range, increasing from  $-10\text{ }^{\circ}\text{C}$  to  $110\text{ }^{\circ}\text{C}$ . For each temperature change, 30 mins waiting time was required to achieve a stable state. Voltage and current measurements were described on subsection 2.2. Experimental test was carried out under DC voltage excitation, considering that the conduction property (i.e. dominant at static regime) is strongly temperature dependent.

Also, dielectric spectroscopy can be investigated under temperature range from  $-10\text{ }^{\circ}\text{C}$  to  $110\text{ }^{\circ}\text{C}$ , thanks to a cryogenic controller (ITC503). To create the low temperature, liquid nitrogen was employed by placing it in a vacuum chamber driven by a vacuum pump.

### 2.4. Mechanical characterization

Experimental monotonic tensile testing was applied to evaluate the mechanical properties of the ZnO/PDMS composites. Based on linear elastic behavior, defined by stress-strain relationship, it was possible to define the Young modulus of the materials [9]. The samples are cut into around  $30 \times 2\text{ mm}^2$  stripes and fixed with two boundaries of Shimadzu TCE-N300 load frame. A ramp-up tensile load at rate of  $0.1\text{ mm.s}^{-1}$  was applied to a uniaxial stress-strain pattern. The composites were subjected to an increasing force until breakdown occurs. This test allowed to determine the ultimate tensile strength ( $T_{\text{max}}$ ) that the material can withstand while being stretched before breaking. Sampling frequency of 100 Hz was chosen to acquire and record both displacement and force signals, which enable to infer the stress and the strain data.

## 3. Results and discussion

### 3.1. Material morphology

In order to evaluate and compare the particles distribution of aligned and random ZnO/PDMS composites, SEM analyses were carried out using a scanning electron microscope (FlexSEM 1000 II, HITACHI). Figure 1 displays the SEM image of specimens with a volume fraction increasing from 10% to 40%, and the particles dispersion is either random or aligned.

For the non-aligned 0-3 samples, ZnO particles were randomly distributed within PDMS polymer matrix, implying a homogeneous dispersion of samples. Inversely, an anisotropic spatial arrangement of reinforced particles was clearly visible in case of the aligned composites treated with dielectrophoresis. It is noticed that the lower the filler content, the easier the alignment effect can be observed [29]. For instance, in case of the 10% vol. 1-3 composite, particles have enough space to create chain-like structure along the field direction. When the filler content is increased, inter-chain interactions are getting stronger

and compete with their interaction with the external field. Consequently, that chains tend to merge together to form a network-like structure, due to greater impact of interactions between particles, caused by their smaller distances. In other words, this behavior is attributed to the fact that at high density composite, interactions between laterally adjacent particles overwhelms the dielectrophoretic force [14]. Consequently, in the 30% and 40 % aligned samples, observation of particle alignment is not evident with respect to the one of 10% and 20%.

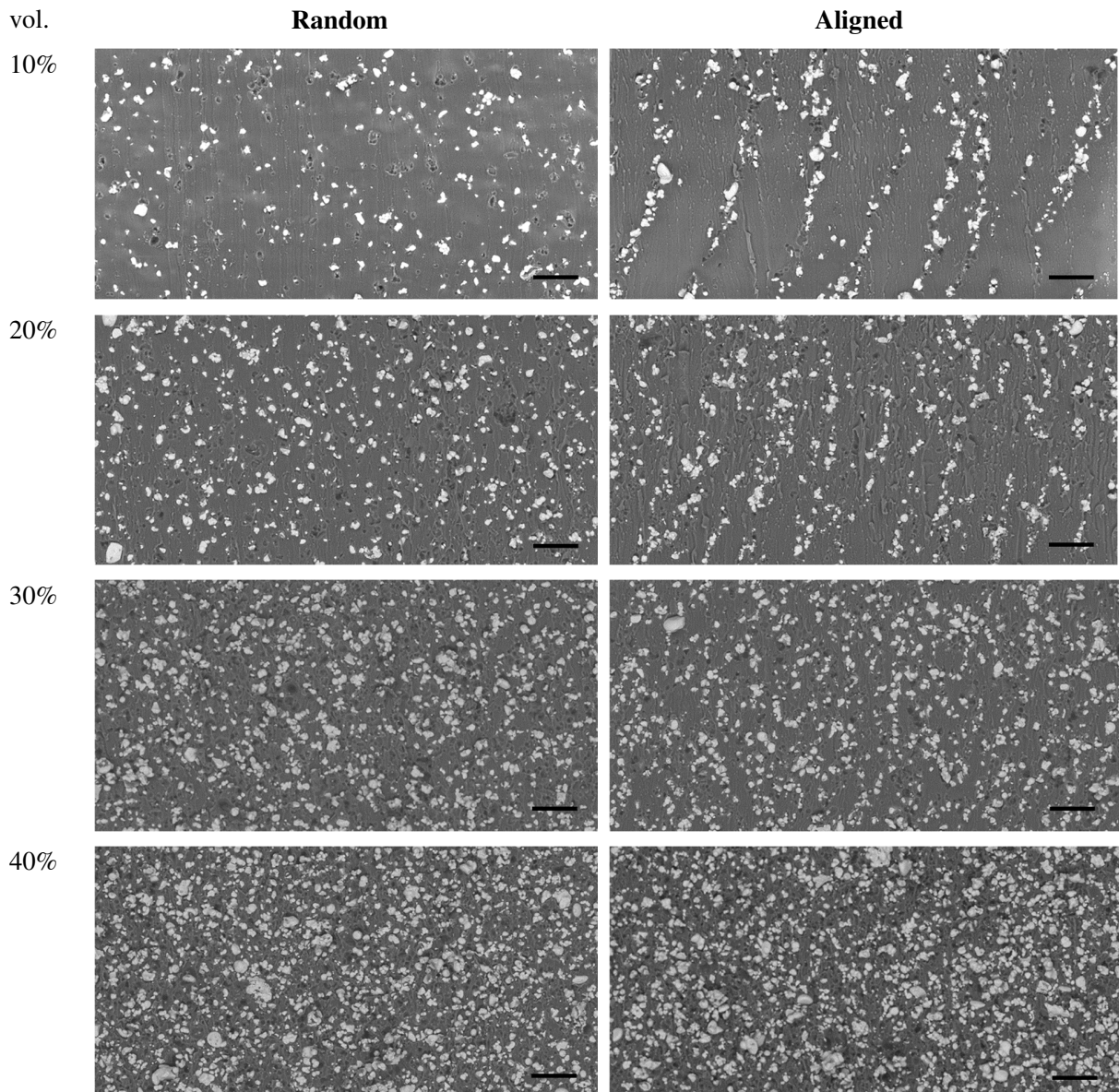


Figure 1. SEM images of random and aligned samples at different volume fraction (the scale bar is of 400  $\mu\text{m}$ ).

### 3.2. Electric field distribution based 2D COMSOL model

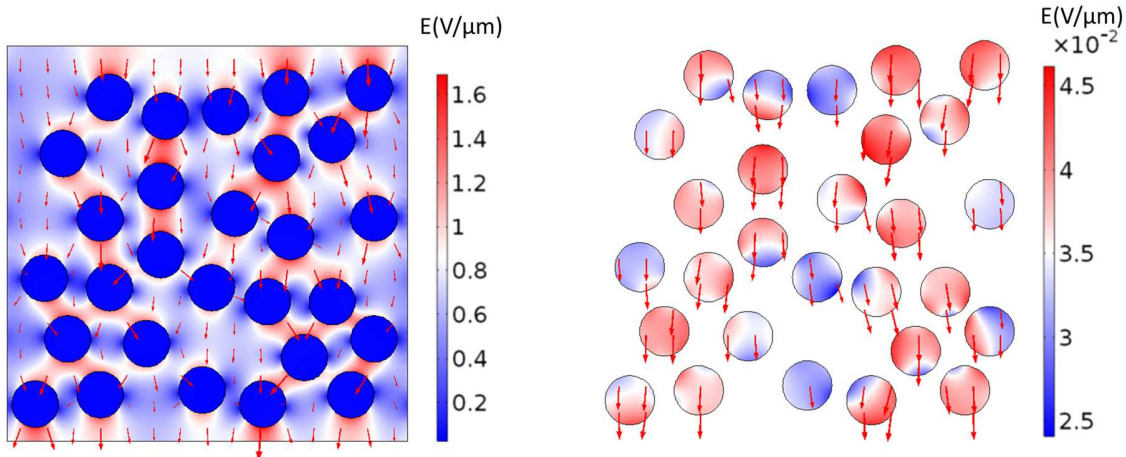
In order to have an idea about the distribution of the field within the particles and its surroundings, 2D COMSOL model is carried out. In the FEM simulation, ZnO circular particles with a diameter of 10  $\mu\text{m}$  are defined, embedded in PDMS polymer with 80  $\mu\text{m}$  long  $\times$  70  $\mu\text{m}$  wide. The bottom of the matrix is

electrical ground whereas a potential is applied on the top, allowing to drive an electric field to the whole matrix. In this study, two different levels of electric field are chosen, i.e.  $0.5 \text{ V}/\mu\text{m}$  and  $2 \text{ V}/\mu\text{m}$ . Under low electric field, the ZnO particles are dielectric isolation as their applied electric field is under the switching value. On the other hand, when the electric field exceeds the switching value, ZnO becomes conductor, leading to drastically increase current through the samples.

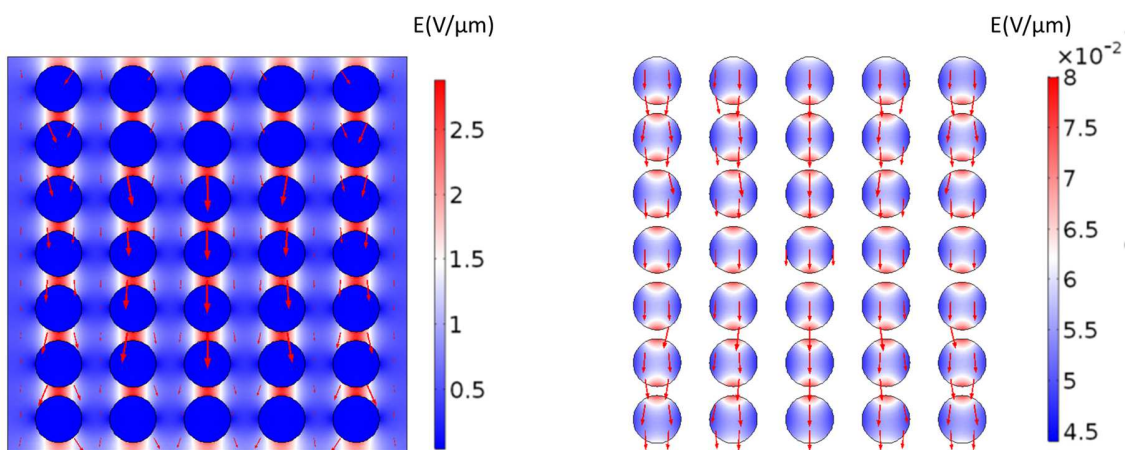
Several studies have been investigated to characterize the electrical properties of ZnO material whose properties strongly depend on level of the input field. In [30], current-voltage characteristics of a photo-conducting organic liquid-crystal film based Zinc octakis (b-decoxyethyl) porphyrin (i.e. ZnODEP) was performed, allowing to deduce the electric field threshold of around  $0.15 - 0.2 \text{ V}/\mu\text{m}$ . Alternatively, Ahmad *et al.* demonstrated that under low applied electric field, the relative permittivity (real part) of the ZnO powder was constant, and then drastically drop when the electric field attains the threshold value (i.e., approximately  $0.15 - 0.9 \text{ V}/\mu\text{m}$ ) [31]. Actually, in a classical capacitor made of dielectric material, the high conductance causes internal leakage of the capacitor, resulting in lower capacitance [32]. Under low applied electric field, ZnO composite behaves as a typical dielectric material, which contains two main components (capacitive and resistive). In that case, the capacitive component is considered to be dominant, as low conduction current is observed. On the other hand, when being subjected to increasing electric field that exceeds the percolation threshold, the current density flowing through the material drastically increases, and the material acts like resistor rather than capacitor [33]. This confirms the semiconductor behavior of ZnO composite, which can be employed as microvaristor system. A lot of studies investigated on current-voltage characteristics of ZnO composites, but none of them has yet investigated on their electric-field dependence where several effects would appear simultaneously. The next subsection will clearly address this issue.

Preliminary COMSOL model results illustrate the electric field distribution in random and structured micro-composites with a concentration of 30% vol. Two different amplitudes of electric field are used, i.e.  $0.5 \text{ V}/\mu\text{m}$  (Figure 2 a-b) and  $2 \text{ V}/\mu\text{m}$  (Figure 2 c-d). The results in Figure 2 a-b confirm that whatever the material configuration (0-3 or 1-3), the ZnO particle is a dielectric isolation, as the electric field driven within the particles is significantly lower than the switching value ( $\sim 0.2 \text{ V}/\mu\text{m}$ ). On the other hand, under higher input excitation (cf. Figure 2c-d), ZnO passes from isolator to conductor, which is the reason of much higher electric field affecting to the particles (i.e., excess the switching value). In the 1-3 materials (Figure 2 b and d), as the axes of the particle chains are oriented perpendicular to the active surface (i.e., applied by an electric potential), the electric field would mainly affect the interparticle interactions within the same chain. This leads to homogenous electric field distribution of all particles, which is contrary to the case of the 0-3 matrix (Figure 2 a and c). Interestingly, when the composite is subjected to an intermediary level of  $1 \text{ V}/\mu\text{m}$ , the aligned particles become conductor whereas the random ones are still isolator, as its switching field is superior to the one of the 1-3 matrix.

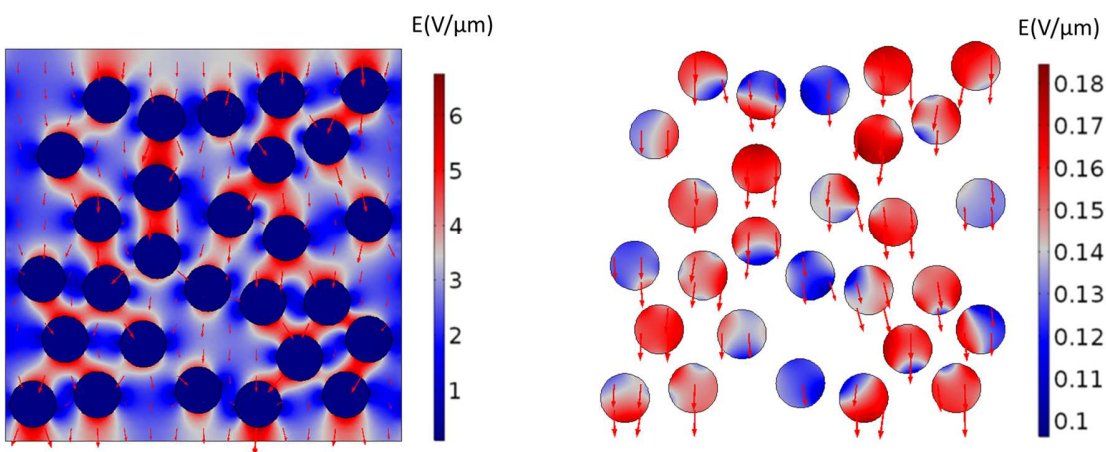
Regardless the structure of the samples (0-3 or 1-3), the electric field level is greatly higher in the polymer matrix than in the particles, especially around the particles, the electric field becomes maximum. This result is consistent with the one of Pedroli *et al.* [34], where the electric field is always more significant in the material with lower dielectric permittivity (in polymer, for instance).



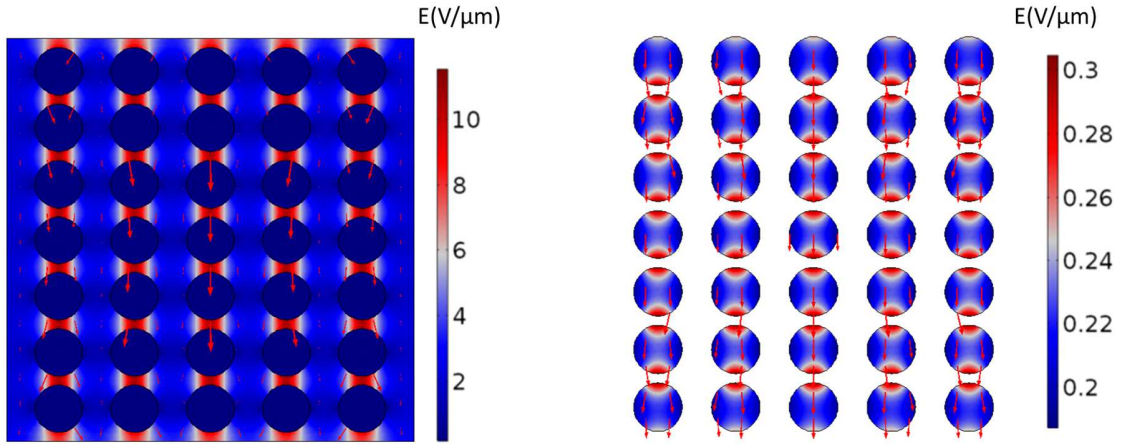
a) Random ZnO/PDMS composite excited by  $0.5 \text{ V}/\mu\text{m}$



b) Structured ZnO/PDMS composite with  $0.5 \text{ V}/\mu\text{m}$



c) Random ZnO/PDMS composite excited by  $2 \text{ V}/\mu\text{m}$



d) Structured ZnO/PDMS composite with 2 V/μm

Figure 2. Electric field distribution in random and structured micro-composites with 30% volume fraction (on the left-hand side), and a closer view of the particles (on the right-hand side).

### 3.3. DC current density – electric field characterization

This section aimed to show the nonlinear current density – electric field (J-E) characteristics of both 0-3 and 1-3 ZnO/PDMS composites doped with different filler concentrations. To obtain a point-to-point curve, all samples are subjected to a number of DC voltage levels until they reached the switching value. It will be shown that any increment voltage beyond the switching value promotes large conduction current flow in the materials. In this test, the amplitude of applied electric field was limited at 2 V/μm so as to avoid initiation of breakdown, which eventually caused damage to the test samples. For each measured point, after a 10 mins waiting, current across the sample attained the steady state that was measured through the current amplifier. For a better visualization of the isolator-semiconductor transition, which is situated around the percolation threshold characterized by the switching field, different samples subjected to different fields are displayed in the J-E curve. Actually, the percolation depends on the sample's concentration and structuration (0-3 or 1-3 connectivity).

Figure 3 explains how the nonlinear conduction behaviors vary with the filler concentration. As reported by Yang *et al.*, this issue can be justified by considering influence of the conduction path made by ZnO/ZnO connectivity [35]. When the filler concentration is below the percolation threshold, the composite behaves as an insulator. As soon as conduction paths develop above the percolation threshold, the composite manifests nonlinear properties. Some of the conduction paths are mainly straight, while others are curved. The shortest conduction paths are those with the greatest current density, because the conductivity of the paths is the largest [36]. Thus, the main conduction paths are shorter and straighter at higher filler concentrations, leading to lower switching field. Inversely, the conduction paths in low filler concentration are mostly roundabout and curved, because of predominant resistive connectivity between particles and polymer, giving raise to higher switch field. The switching fields ( $E_s$ ) of the composites are shown in Table 1.

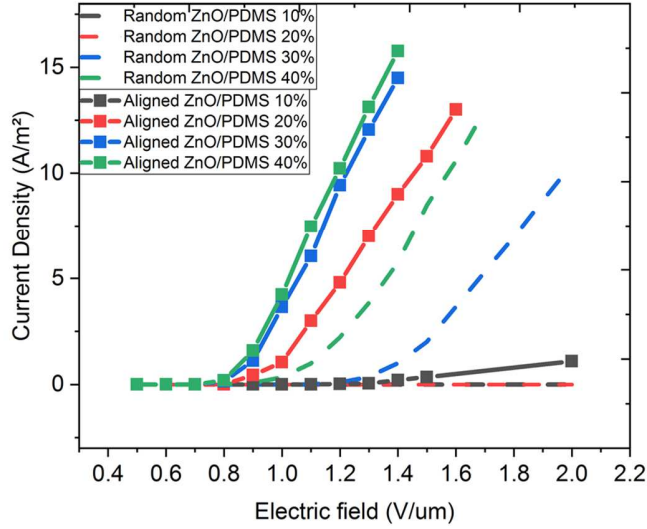


Figure 3. Nonlinear J-E characteristics of random and aligned-ZnO/PDMS composites at filler content of 10%, 20%, 30%, 40%. Dotted lines represent the 1-3 aligned samples whereas dashed line depict the 0-3 random samples.

It is expecting in Figure 3, that whatever the applied electric field, the 0-3 composites with low ZnO content (10% and 20% vol.) always perform as an insulator where no switching field exists. Nonetheless, the 1-3 aligned structures doped with the same concentration allows the creation of the conduction path, being confirmed by apparition of the switching field. The result demonstrates that the dielectrophoretic alignment on ZnO particles successfully enhances the electric response of the composite. For instance, the 1-3 matrix with 20% vol. exhibits higher current density than the 0-3 matrix with 40% vol.

The J-E characteristics described in Figure 3 clearly shows the semi-conductor property of the ZnO composite, which consists of two different slopes: The first slope exhibits very low level, corresponding to the insulating behavior below the switching field. The second slope, on the other hand, drastically increase when the material becomes conductor. In that case, the charge carriers get enough energy to freely move through the material, resulting in significantly enhanced current density. Table 1 shows the conductivity value ( $\sigma$ ) of all samples (except the random composites filled with 10% and 20% where no switching field exists), which is deduced from the second slope. Clearly, the conductivity increases with the increasing filler content. Furthermore, its value is higher in the case of the 1-3 composites compared to the 0-3 ones.

Table 1 describes the nonlinear coefficient  $\alpha$  of random and aligned composites elaborated with ZnO concentration of 10%, 20%, 30%, 40%. The nonlinear coefficient  $\alpha$  is calculated as [37]:

$$\alpha = \frac{\log \frac{J_2}{J_1}}{\log \frac{E_2}{E_1}} \quad (1)$$

where  $J_1$  and  $J_2$  are the measured current densities with amplitude of 1 A/m<sup>2</sup> and 10 A/m<sup>2</sup>, respectively;  $E_1$  and  $E_2$  are the corresponding DC applied electric field. In case of the 10% and 20% random composites, as well as the 10% aligned composite, it is not possible to calculate  $\alpha$  as their current densities cannot go up 10 A/m<sup>2</sup>.

The nonlinear coefficient  $\alpha$  gradually increases with the increasing ZnO concentration, which is attributed to the incremental conduction path in composites. Also, the 1-3 structure favors the nonlinear behavior, leading to 10% increase in the value of  $\alpha$  with respect to the 0-3 matrix. Interestingly, for the 30% and 40% composites with aligned structure or not, the nonlinear coefficients are almost identical. This can

be explained that in such high concentration composites, the amount of active short conduction path almost saturates, and little discrepancy was observed.

Table 1. Nonlinear coefficient ( $\alpha$ ) of random and aligned composites at 10%, 20%, 30%, 40% volume fraction.

	10% <sub>vol</sub>	20% <sub>vol</sub>	30% <sub>vol</sub>	40% <sub>vol</sub>
$E_{s-random}$ (V/ $\mu$ m)	-	-	1.39	1.09
$E_{s-aligned}$ (V/ $\mu$ m)	1.93	0.98	0.88	0.85
$\sigma_{random}$ (S/m)	-	-	1.60E-5	2.05E-5
$\sigma_{aligned}$ (S/m)	-	1.99E-5	2.73E-5	2.87E-5
$\alpha_{random}$	-	-	6.51	6.52
$\alpha_{aligned}$	-	5.96	7.21	7.24

Finally, the shape of the curve described in Figure 3 clearly showed the nonlinear characteristic of J-E curve, which consists in a transition from dielectric to semiconductor behavior. The root cause of the sharp increase in the current density around the switch field could be originated from the charge accumulation on the grain boundaries of ZnO crystals. Due to arrangement of oxygen atoms, Schottky barriers are formed on the grain boundary and a depletion layer is formed within the ZnO grains [38]. Therefore, charges are accumulated in the depletion layers until the Schottky potential barrier is reached, which elaborates the conduction mechanism in the ZnO material [31].

### 3.4. Temperature stability

#### 3.4.1. J-E characteristics under temperature variation

In this section, the influence of temperature on the electric properties of developed materials was investigated. Figure 4 displayed the nonlinear J-E characteristics of the random and aligned composites elaborated with 40% of ZnO content, which were measured at various temperatures in the range  $-10$  °C to  $110$  °C. It can be seen in that for both 0-3 and 1-3 structures, the switching field gradually increases with increasing temperature from  $10$  °C to  $110$  °C. The primary reason is that growing temperature facilitates the contact resistance between the fillers, leading to higher switch field [35]. More specifically, because of the large discrepancy of thermal expansion coefficient between ZnO particles (around  $4.3 \times 10^{-6} K^{-1}$ ) [39] and PDMS polymer (around  $9.6 \times 10^{-4} K^{-1}$ ) [40], the expansion of matrix may block the formation of conduction path and also transform a thin insulation gap into thick gap between ZnO particles. Additionally, enhancing temperature makes the interaction force between fillers increase, resulting in large face contact interfaces and resistance [41]. Therefore, an increment of switching field is expected in composite measured at increasing temperature.

Interestingly, it was observed a decreasing trend of switch field from negative temperature ( $-10$  °C) to positive temperature ( $10$  °C), which may be ascribed to the temperature effect on carrier transport between ZnO particles and segmental mobility of polymer. The energy bandgap of semiconductor tends decrease electron concentration in the conduction band with increasing temperature, resulting in lower switch field and sharper increase in current density when a high voltage is applied [20,42]. Also, the liberation of charge carriers from traps to greater mobility at high temperature improves the conductivity and thereby decreases the switch field [43]. It therefore seems that the increase of carrier transport through the ZnO particles dominates the conductivity of the composites at low temperatures between  $-10$  °C and  $10$  °C, but the increase in contact resistance dominates between  $10$  °C and  $110$  °C. Consequently, the temperature

dependence of the J-E characteristics is a result from two competitive effects, i.e., contact resistance and carrier transport.

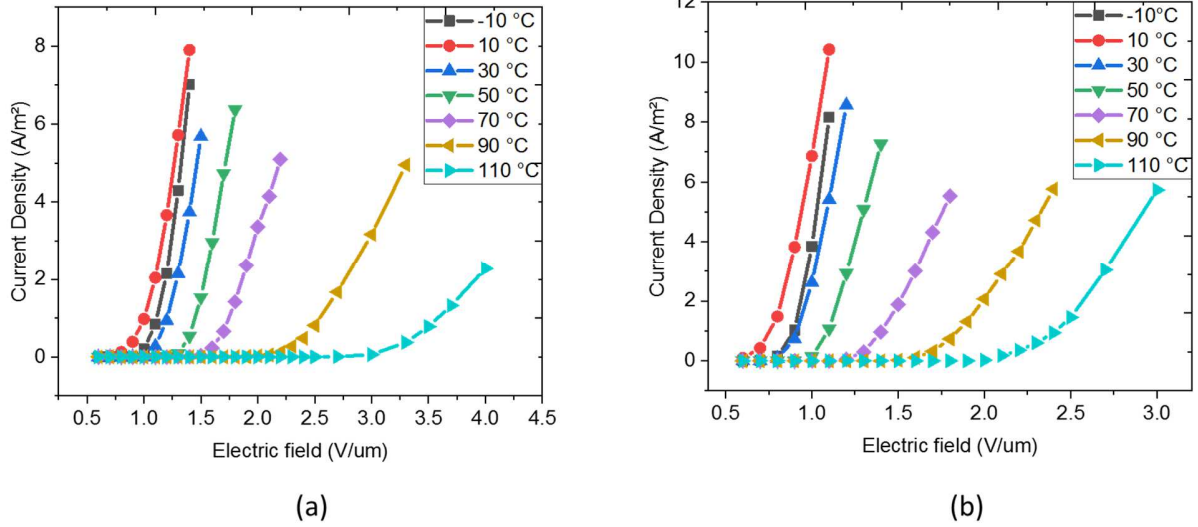


Figure 4. Nonlinear J-E characteristics of (a) random, and (b) aligned-ZnO/PDMS composite with filler content of 40% at different temperatures.

### 3.4.2. Dielectric characterization under temperature variation

Figure 5 showed the temperature dependence of the dielectric constant ( $\epsilon_r'$ ) and the loss tangent with frequency in the range 0.1 Hz–1 MHz. It was pointed out in the previous work that the higher the particle concentration, the higher the broadband dielectric variation [24]. In other words, the frequency-dependent behavior is more observable in the case of ZnO composite filled with 40% vol., as opposed to the other containing lower fraction content. Hence, in this study, the 40% sample is considered be the most representative for temperature-stability analysis of the dielectric properties. For a sake of simplicity, only result of the aligned composite is shown.

As seen in Figure 5 (a), the decrease relative permittivity ( $\epsilon_r'$ ) with increasing frequency at a given temperature is related to dielectric relaxation of polymer [44,45]. Specifically, this behavior can be explained by the fact that at high frequency, dipoles are not sufficiently rapid to orient themselves, provoking a lag between the oscillating dipole and the applied field dynamics [46,47]. Nonetheless, at low frequency, high  $\epsilon_r'$  value is probably originated from the interfacial polarization induced by large discrepancy in the permittivity of ZnO and PDMS matrix. Meanwhile, the dielectric loss ( $\tan\delta$ ) decreases rapidly within low frequency range, which is due to the free charge motion within matrix based on hopping contribution [48,49]. On the other point of view, Aldar *et al.* [50] stated that such a behavior was originated from the basis of space charge polarization, i.e. dedicated to the Debye-type dielectric dispersion. It was pointed out by Macdonald [51] that the internal electric field induced by the space-charge polarization became so inhomogeneous that the field intensity near electrodes was very high while midway between electrodes was nearly zero. This causes the localized accumulation of charges under the applied external field and thereby enhancing the space charge polarization. Interestingly, the dielectric loss is stable between a frequency range of [50 Hz ,100 kHz]. On the other hand, an upward trend occurs at higher frequency (i.e. beyond 100 kHz), which is ascribed to the relaxation of dipolar orientational polarization [52–54]”. It is revealed in Figure 5 (b) that a peak in the  $\tan\delta$  loss might be observed beyond 1 MHz, i.e., similarly to the one reported in [55]. Generally, dipole relaxation in a dielectric material (e.g. PDMS) is undesirable for capacitor applications because this process is usually accompanied by great variations in permittivity ( $\epsilon_r'$ ) and  $\tan\delta$ .”

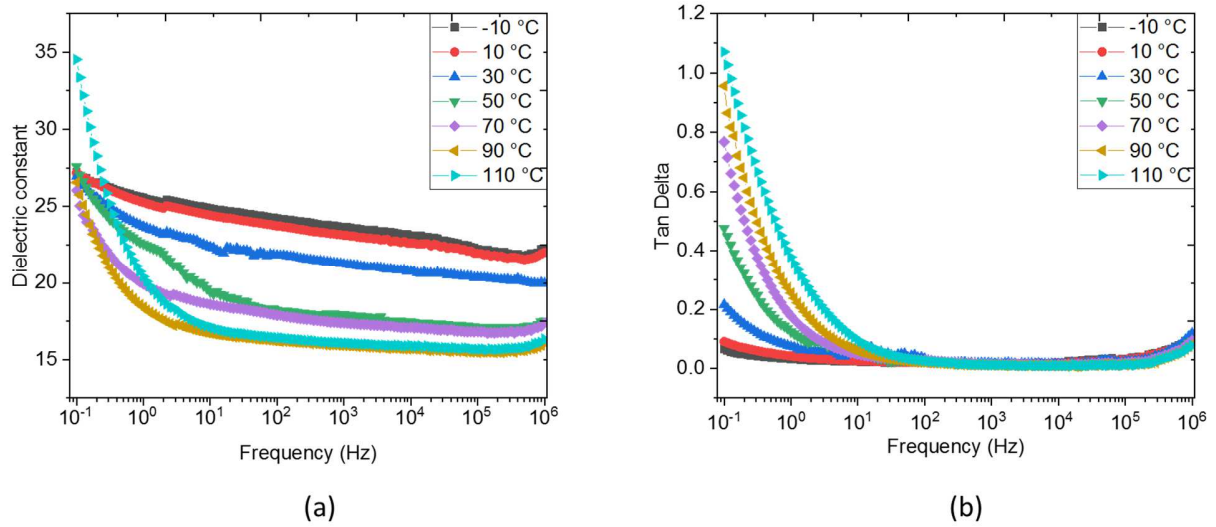


Figure 5. Broadband dielectric spectroscopy including (a) dielectric constant, and (b) dielectric loss tangent of the 40% vol. aligned samples at different temperature.

Regarding the dielectric characterization under temperature variation of a typical dielectric composite, Ramajo *et al.* and Hadik *et al.* identified three major mechanisms [56,57], that can be cited as following:

- 1) The dielectric response of the filler is temperature dependent, which is due to the changes in the filler structure (below Curie temperature). It has been reported that the dielectric properties of semiconductor/polymer composites are greatly affected by the conductivity of fillers. In other words, dielectric constant of the composites enhances with respect to an increase in the filler's conductivity. As a result, the dielectric constant of semiconductor fillers usually increases with the increase of temperature [58].
- 2) The segmental mobility of polymer with temperature: The higher the temperature, the greater the freedom of the dipole molecular movement. This leads to improvement of dielectric constant.
- 3) The contact between the ZnO particles is interrupt due to the thermal expansion of PDMS matrix, results in decrease in electrical conductivity, thus reducing the dielectric constant.

Under an excited electric field, particles of ZnO in micro size act as dipoles and obtain high freedom of movement to reach high dielectric constant [59]. However, as the applied input voltage is relatively small (i.e. 1.4V amplitude, corresponding to 2-3 mV/ $\mu\text{m}$ ), enhancing in both dielectric constant ( $\epsilon_r'$ ) and electrical conductivity with increasing temperature can be neglected. Thereby, the decrease trend of  $\epsilon_r'$  with temperature in Figure 5 would be mainly affected by the dielectric properties of PDMS or the interaction between two constituent phases. On one hand, at a high temperature, the interruption of the conduction path in ZnO/PDMS composite makes it difficult for dipoles to arrange at a certain direction when subjected to electric field. On the other hand, increasing the mobility of dipole molecular chain of PDMS polymer with temperature could favor the dielectric constant, to some extent. Based on the result of Figure 5, it is possible to conclude that the main reason of the dielectric characterization under temperature variation is mainly attributed by the thermal expansion of PDMS matrix. Eventually, similar observation is reported in the literature, where the dielectric constant of PDMS decreases with increasing temperature, i.e. above its glass transition temperature (175 °K) [60].

It has been demonstrated in Figure 5 (b) that at low frequency, the dielectric loss tangent increases as a function of the temperature, whereas almost unchanged at higher frequency. Actually, increasing temperature at low frequency favors segmental mobility of polymer as well as the friction of the rotating dipoles. Also, it makes the degree of dipole orientation increase, causing increase dielectric loss [47]. Interestingly, at the highest temperature (especially 110 °C), the dielectric constant is more prominent at

very low frequency (i.e., 0.1Hz), which is possibly induced by enhanced free-charge displacement under applied electric field. This phenomenon probably stems from the interface polarization of polymer, where an increase in temperature could improve the dielectric constant ( $\epsilon_r'$ ) by facilitating the polarization process. It is worth noting that the estimation of ( $\epsilon_r'$ ) via Solartron is less accurate for the sample measured at 110°C, as its  $\tan\delta$  value is higher than 1. Actually in reality, the permittivity of the sample subjected to 110°C should be smaller and somehow close to the one with other temperature conditions. This is a limitation of Solartron spectrometer, where measurement in the relative permittivity is problematic with a bad dielectric material (i.e. high conduction loss with  $\tan\delta > 1$ ).

### 3.5. Time-varying electric field characterization

The main feature differentiated the ferroelectric materials from the dielectric materials is the presence of spontaneous polarization, retaining the intrinsic electrical polarization in the absence of external field. Thus, the ferroelectricity can be characterized by measuring the intersection of the D-E hysteresis loop with the electric displacement axis, denoted as remnant polarization in response to a high AC electric field [61]. For the dielectric film, when being doped with impurities the dielectric has a finite resistivity, leads to a leakage current. If applying a varying electric field on the composites, the electric energy losses can be divided into two parts: dissipation of dielectric energy from pure dielectric material, and energy losses associated with leakage current inducing from dopant fillers [62]. From a practical application viewpoint, energy loss may cause significant heat generation in electromechanical devices under strong field driving condition, leading to device failure [63]. This subsection aims to distinguish different losses mechanisms of ZnO composite, at the same time to verify the piezoelectricity and semiconductor of ZnO particles. Tests are performed under a large range of electric field, with two configurations comprising bipolar and unipolar polarizations.

#### 3.5.1. Bipolar polarization

For investigating the current density-to-electric field (J-E) characteristics, a sinusoidal electric field with frequency of 1 Hz and amplitude increasing from 0.2 V/ $\mu\text{m}$  to 1 V/ $\mu\text{m}$  were applied to the ZnO/PDMS composites. The measured total current density ( $J_{tot}$ ) through the ZnO/PDMS composite can be decomposed into three components: conduction ( $J_{con}$ ), dielectric ( $J_{die}$ ), and ferroelectric ( $J_{ferro}$ ) [64].

Figure 6 displays the J-E hysteresis loops of both random and aligned ZnO composites elaborated with the same volume fraction. For a sake of simplicity, only those filled with 20% vol. of ZnO were presented. Under a maximum amplitude of 1V/ $\mu\text{m}$  delivered by an external high-voltage source, these samples were revealed to be the most appropriate choice to better highlight the dielectrophoresis effect. As indicated in Figure 6 (a), the 0-3 matrix exhibits a near-capacitive behavior for a whole range of the applied electric field, which is confirmed by a circular-shaped J-E curve. It is generally believed that the dielectric current density ( $J_{die}$ ) has circular relationship with the electric field while the conduction one ( $J_{con}$ ) exhibits a linear response relating to Ohm's law. Concerning the aligned composite shown in the Figure 6 (b), a transition from capacitive to conductive behavior is observed with increasing electric field, which is proven by the disappearance of the circular-shape. Beyond the switching field, the resulting current intensity drastically enhances, reflecting the semiconductor properties of the ZnO materials. As demonstrated by COMSOL simulation (cf. subsection 3.2), the aligned particles are driven by higher field level than the random particles. This justifies why the 1-3 structured composites exhibits lower switching voltage than the 0-3 isotropic sample. Consequently, dielectrophoresis of the ZnO/PDMS composite improves the probability of forming conduction paths, thereby increasing the electrical conductivity of material.

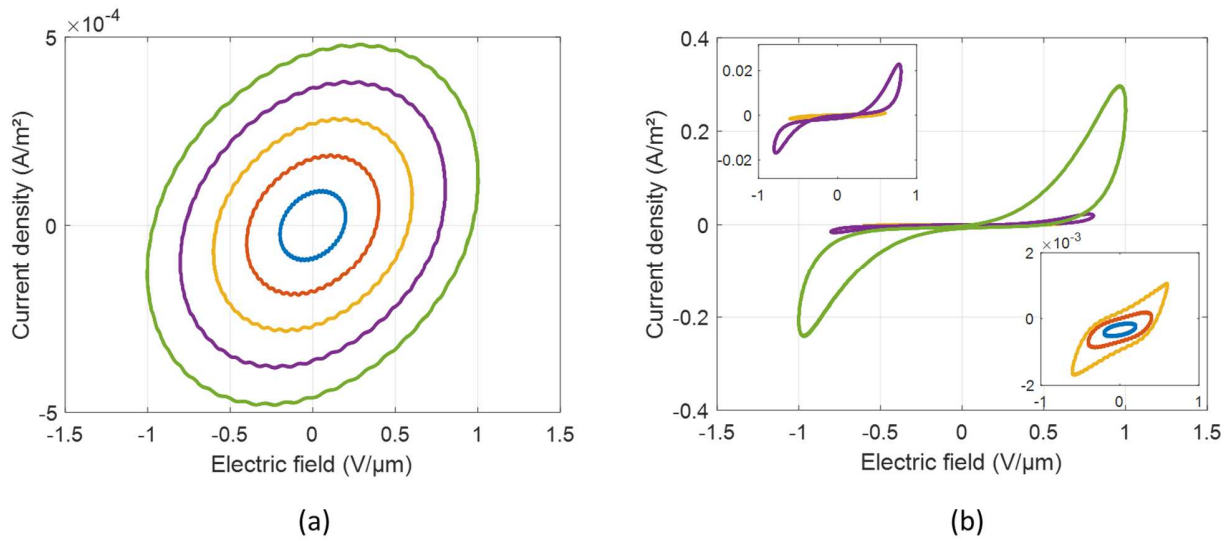


Figure 6. Representative current density vs. electric field of (a) random composite; and (b) aligned composite. Both samples are filled with 20% vol. of ZnO microparticles and are subjected to different levels of electric field.

Figure 7 (a)-(b) illustrates the variation of J-E hysteresis loop for the 0-3 and 1-3 ZnO/PDMS composites elaborated with various concentrations (i.e. 10%, 20%, 30%, and 40%) under a given electric field of  $0.4 \text{ V}/\mu\text{m}$  amplitude. This value is chosen in order to ensure that either aligned or random samples behave as quasi-capacitive like structure, allowing to easier identify the three components of current density ( $J_{con}$ ,  $J_{die}$ , and  $J_{ferro}$  [64]). As expected, higher ZnO particles content leads to superior J-E slope. Actually, the conductivity and dielectric of these materials are boosted, giving raise to enhanced  $J_{con}$  and  $J_{die}$ . A comparison between Figure 6 (a) and (b) clearly shows that the aligned samples exhibit higher current density as opposed to those randomly dispersed. This result is in consistent to the one performed in subsection 3.3.

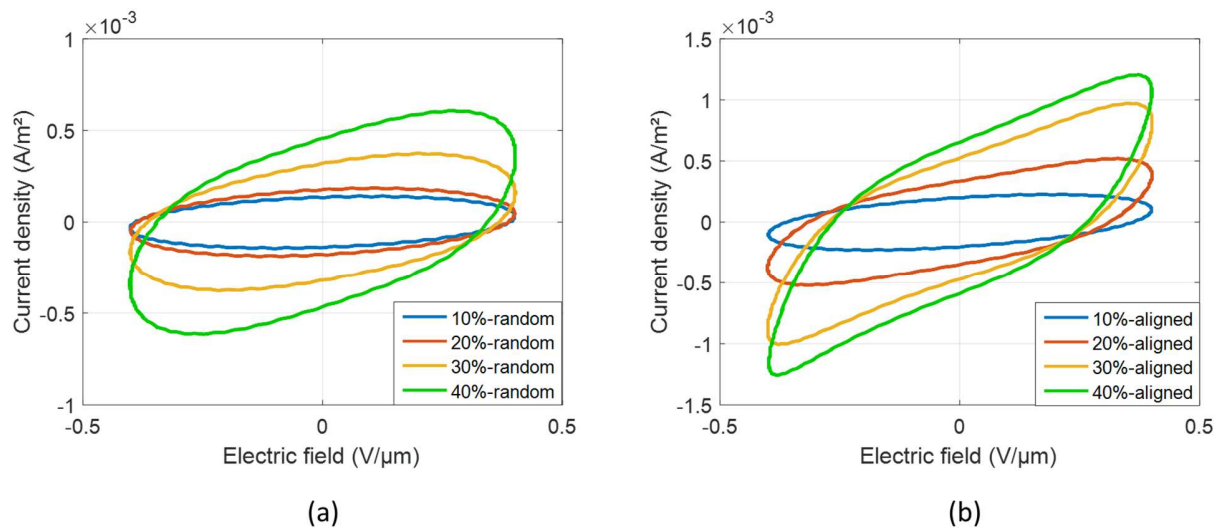


Figure 7. Hysteresis current density loops for ZnO/PDMS composites of different concentrations (a) without and (b) with dielectrophoretic alignment. All samples are excited by the same amplitude of electric field.

In order to further explore the mechanism inside the ZnO/PDMS composite under varying electric field, a simple way to estimate the permittivity and conductivity is introduced. The conduction mechanisms in the dielectric film can be divided into electro-limited conduction, which depends on electrode-dielectric contact, and bulk-limited conduction relating to the dielectric itself [20]. In this case, for simplification only bulk-limited conduction mechanisms are considered. Among them, the capacitive current ( $J_{die}$ ) is assumed to be more dominant than the Ohmic conduction current ( $J_{con}$ ) under low voltage application. In addition of these current densities, ferroelectric property of ZnO fillers should be getting involved ( $J_{ferro}$  [64]). Taking 40% vol. of aligned sample as a typical example, the analysis result depicted in Figure 8 consists of several steps:

- Firstly, as shown in Figure 8 (a), the conduction current density  $J_{con}$  is extracted and assumed to be linear to the electric field ( $E$ ) according to the Ohm's law. The electrical conductivity ( $\sigma$ ) can be inferred from:

$$J_{con} = \sigma E \quad (2)$$

- Secondly, the charge density or the polarization ( $D_T$ ) can be determined by integrating the current density over time after subtracting the conduction element. The polarization only consists of the dielectric ( $D_{die}$ ) and ferroelectric properties ( $D_{ferro}$ ) that can be expressed as:

$$D_T = D_{die} + D_{ferro} = \int (J_{tot} - J_{con}) dt \quad (3)$$

Figure 8 (b) describes the linear polarization-versus-electric-field (D-E) characterization, allowing to conclude that the relative permittivity ( $\epsilon_r$ ) is almost constant under low input voltage range. Considering the dielectric loss factor (denoted as  $\epsilon_r''$ , the imaginary part of  $\epsilon_r$ ) is negligible, only the real part of  $\epsilon_r$  (denoted as  $\epsilon_r'$ ) is taken in consideration. In other words,  $\epsilon_r'$  attributed to the dielectric charge ( $D_{die}$ ) can be obtained by fitting with the following linear model:

$$D_{die} = \epsilon_0 \epsilon_r' E \quad (4)$$

Therefore, a relative permittivity approximately 30.87 for the 40% vol. aligned composite is derived, which is perfectly in agreement with the one measured via the Solartron (cf. subsection 3.4.2). It is noteworthy that the polarization ( $D_T$ ) displays very small hysteresis area, demonstrating poor ferroelectric property of the ZnO composite.

- Thirdly, the fitted polarization  $D_{die}$  can be subtracted from the total polarization, allowing to draw the ferroelectric polarization ( $D_{ferro}$ , yellow line in Figure 8 (b)). The remnant polarization, corresponding to the  $D_{ferro}$  value when the electric field turns back to zero, is very closed to zero, confirming the weak piezoelectric effect of the ZnO material. This result agrees with the previous work [24], where the piezoelectric sensitivity of ZnO composite ( $d_{33} \approx 0.5 \text{ pC} \cdot \text{N}^{-1}$ ), despite its optimized configuration (high particle concentration, good anisotropic structure through dielectrophoresis), is dramatically smaller than the one of the conventional counterparts like PZT ( $d_{33} \approx 20 \text{ pC} \cdot \text{N}^{-1}$ ) [65] or BaTiO<sub>3</sub> ( $d_{33} \sim 5 \text{ pC/N}$ ) [66].
- Lastly, the dielectric current and ferroelectric current densities are carried out through the gradient of the capacitive polarization ( $\frac{dD_{die}}{dt}$ ) and the ferroelectric polarization ( $\frac{dD_{ferro}}{dt}$ ), respectively shown in the Figure 8 (a). Figure 8 (c)-(d) describes the time varying behavior of the electric field together with the resulting current density, and the charge density. On one hand, the electric field lags the current density, which is correlate to the dominant capacitive property represented by the circular-shaped J-E curve. On the other hand, the electric field and the charge density are in-phase, confirming linear relationship between  $D_T$  and E.

It is worth noting that using experimental measurement to derive three unknown parameters, even with the advantages of fitting it with analytical model, leads to inevitable errors. Especially for the material with low ferroelectricity like ZnO, i.e., generally considered non-ferroelectric. However, the

purpose here is not to accurately quantify the ferroelectricity level of ZnO composite, which is usually characterized by estimating the remanent polarization based on ferroelectric-current-versus-electric-field loop [64]. The objective involves in using the resulting D-E hysteresis responses as a qualitative indicator to confirm the piezoelectric behavior of the developed composites. As suggested, small hysteresis in ferroelectric polarization loop clearly manifests low piezoelectricity, which in turn makes it difficult and challenging to extract the ferroelectric current in comparison with the other dominant current components (leakage and capacitive). Accordingly, to confirm in a more rigorous manner the ferroelectric properties of ZnO composite, we designed in previous work a special experimental setup to measure the piezoelectric charge coefficient with a higher sensitivity [24].

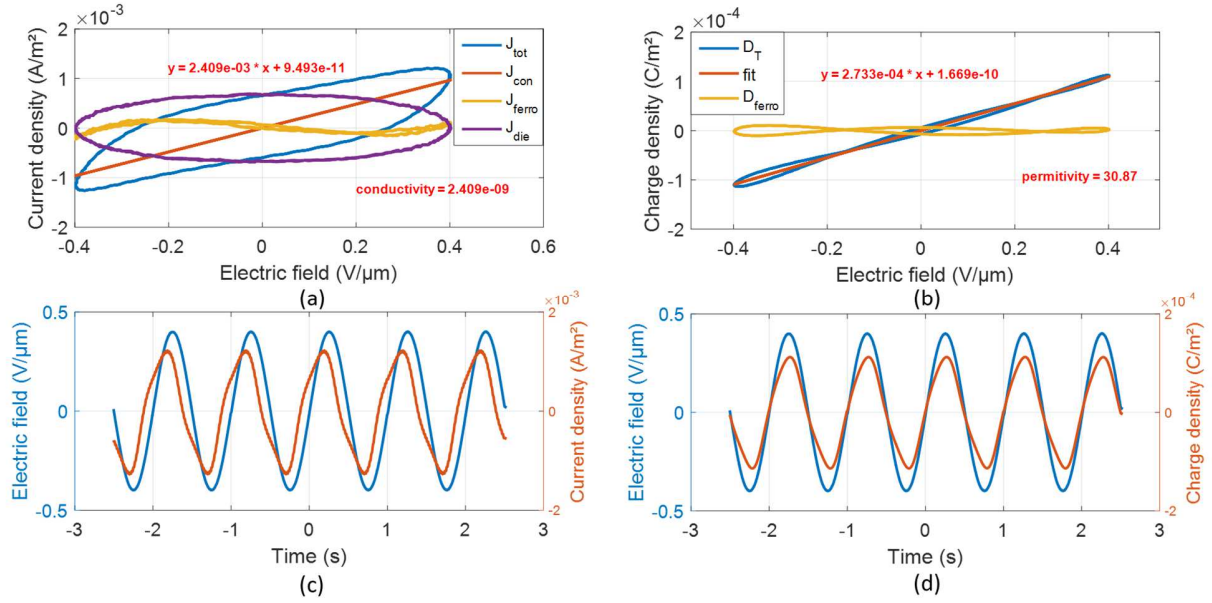


Figure 8. Electrical characterization of the 40% vol. aligned ZnO/PDMS composite under input electric field of 0.4 V/μm amplitude. (a) Decomposition of the total measured current densities into three components ( $J_{con}$ ,  $J_{die}$ , and  $J_{ferro}$  [64]), the conductivity is deduced using the Ohm's law. (b) Polarization loop of charge density versus electric field, allowing to determine the dielectric permittivity and ferroelectric properties of the composite. Time evolution of electric field and resulting (c) current density, and (d) charge density.

The relative permittivity and the electrical conductivity of the 0-3 and 1-3 composites at different ZnO content have been calculated and summarized in Table 2. Clearly, the higher the volume fraction of ZnO, the better the relative permittivity and the conductivity. Meanwhile, an improvement of the permittivity assigned to the introduction of ZnO/ZnO interface polarization has been achieved with the 1-3 matrix. Furthermore, a substantial increase of 3 to 6 times in the conductivity resulted from enhanced short-conducting paths were observed for the composite embedded with aligned ZnO particles.

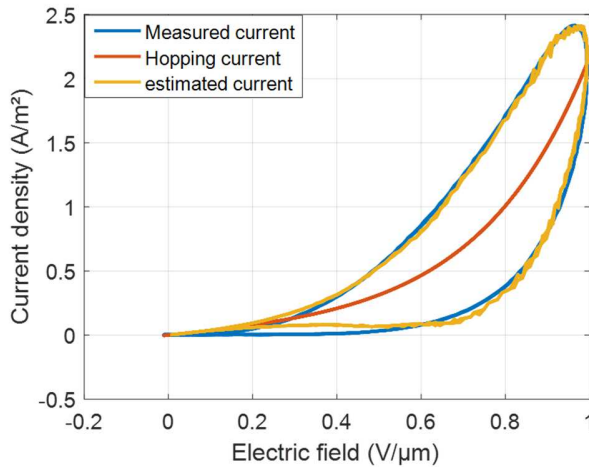
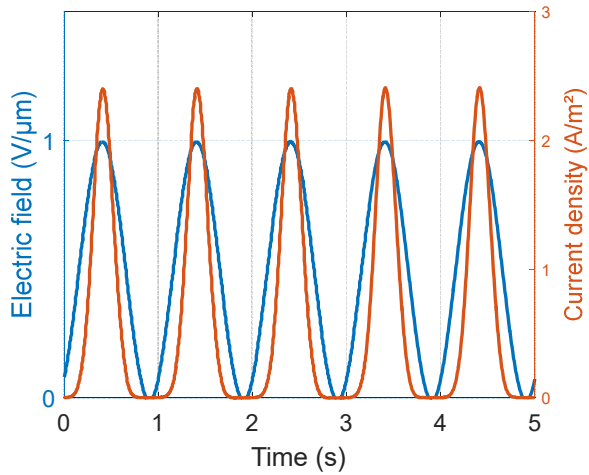
Table 2. Calculation results for random and aligned ZnO/PDMS at different filler concentration.

Volume fraction	$\epsilon_{random}$	$\epsilon_{aligned}$	$\sigma_{random}$ (S/m)	$\sigma_{aligned}$ (S/m)
10%	6.16	9.34	0.397E-10	2.442E-10
20%	8.05	17.01	1.153E-10	8.594E-10
30%	15.07	25.52	3.924E-10	18.69E-10

<b>40%</b>	22.56	30.87	8.281E-10	24.09E-10
------------	-------	-------	-----------	-----------

### 3.5.2. Unipolar polarization

This subsection dealt with the nonlinear J-E curve of the 1-3 aligned composite elaborated with 40% ZnO concentration, which were powered by a high input voltage with 1 Hz frequency. To further investigate the electric response where the ferroelectric behavior was excluded, a positive sinusoidal wave (unipolar) was used. The electric field amplitude was chosen to be equal 1 V/ $\mu\text{m}$  (i.e., above the switching field), at which the conduction mechanism turned to be the dominant component with respect to the capacitive one. This property is confirmed by Figure 9 (a) where no phase shift between current and voltage has been observed. The material behaves as a semiconductor that enables the flow of current as soon as the electric field is above the switching value. The unipolar polarization loop of the 40% vol. aligned samples was displayed on Figure 9 (b), clearly reflecting its nonlinear J-E characteristics. The results point out a significant hysteresis curve caused by dielectric losses, which is drastically increase with the voltage level. The following analysis will clarify this issue.



(a)

(b)

Figure 9. Nonlinear J-E characteristics of the 1-3 ZnO/PDMS composites (40% volume fraction) that is powered by a high unipolar voltage at 1 Hz frequency and 1 V/ $\mu\text{m}$  amplitude. (a) Time evolution of current density and electric field. (b) Experimental measure and theoretical model of J-E curve. The measured current density (blue) is compared to the estimated one (yellow), which is the sum of the hopping current density (red) and the dielectric current density.

The measured total current density ( $J_{tot}$ ) is supposed as the sum of the conduction current ( $J_{con}$ ) and the dielectric current ( $J_{die}$ ):

$$J_{tot} = J_{con} + J_{die} \quad (4)$$

The conduction current density appearing within the sample is essentially attributed by the tunneling effect of trapped electrons between the particles when a relatively high electric field was applied. This effect can be described according to the hopping conduction model [20,67]:

$$J_{con} \approx J_{hopping} = A_0 \sinh\left(\frac{E}{A_1}\right) \quad (5)$$

where  $A_0$  and  $A_1$  are the constant factors that are given by:

$$A_0 = J_0 \exp\left(\frac{-E_a}{kT}\right) \quad (6)$$

$$A_1 = \frac{2kT}{aq} \quad (7)$$

where  $J_0$  is a constant current density,  $E_a$  is the activation energy from trap states to the bottom of conduction band;  $a$  is the meaning distance between trap sites;  $q$  is the charge carrier constant;  $k$  and  $T$  are the Boltzmann constant and the temperature, respectively. When continuous paths are formed, that is, above the percolation threshold, the  $J_{con}$  characteristics are Ohmic if the electric field across the barrier is lower than  $A_1/2$  [68].

Table 3 shows the values of  $A_0$  and  $A_1$  fitted from the hopping model under a 1 V/ $\mu\text{m}$  external electric field, which is performed on aligned samples with various ZnO faction content. Interestingly,  $A_0$  increases as the concentration of the ZnO phase increases, and tends to be saturated at a fraction content of above 30%. This indicates that the distribution of the conducting particles in the composite and the activation energy ( $E_a$ ) behavior are intimately connected. Indeed, on average, larger volume fractions entail shorter tunneling distances, so that hopping between neighboring conducting particles, even in the presence of some activation energy, becomes increasingly favorable. In other words, such an effect is facilitated in composites with large conducting particles or aggregates because of the lower activation energies participating in the hopping processes. Above the percolation threshold, the activation energy decreases when the fraction of particles increases, and it also depends on temperature [68]. Indeed, the activation energy decreases with decreasing temperature and at very low temperatures, conductivity becomes temperature independent.

On the contrary,  $A_1$  shows little dependence on the concentration of ZnO particles. It can be assumed that when the filler concentration increases,  $A_1$  stays at balance state between two contrary effects: 1) the increasing trend of the charge carrier concentration attributed from the ZnO conduction path, and 2) the decreasing trend of the average trap distance. The addition of particles tends to obstruct the formation of long polymer chain, thus develop more traps in the free space between the polymer chain segments [69].

Table 3. Fitting results of variables  $A_0$ ,  $A_1$  from the hopping model with different samples

Samples	$A_0$	$A_1$
10% <i>aligned</i>	53.822	0.325
20% <i>aligned</i>	163.694	0.2715
30% <i>aligned</i>	313.057	0.2730
40% <i>aligned</i>	301.9108	0.2614

In addition to the conduction hopping current density, the dielectric current density associated to the pure dielectric can be expressed as:

$$J_{die} = \frac{dE}{dt} \varepsilon_0 \times \varepsilon_r(E) \quad (8)$$

where  $\varepsilon_r(E)$  is the relative permittivity as a function of the electric field  $E$ . Generally,  $\varepsilon_r$  can be described as a complex number  $\varepsilon_r^* = \varepsilon_r' - i\varepsilon_r''$ , consisting of a real component  $\varepsilon_r'$  and an imaginary component  $\varepsilon_r''$ . The dielectric loss is defined as the dissipation of electrical energy induced in an alternating electric field due to the movement or rotation of dipoles. At low frequency and high electric field, more free charge motion in the composite causes that  $\varepsilon_r''$  is far larger than  $\varepsilon_r'$ . Hence, Eq. (8) becomes:

$$J_{die} = -\frac{dE}{dt} \varepsilon_0 \times i\varepsilon_r''(E) \quad (9)$$

where  $i$  is the imaginary number. In the sinusoidal regime,  $\frac{dE}{dt} = i\omega E$ , which allow to infer that  $J_{die}$ ,  $J_{tot}$ , and  $E$  are perfectly in phase. This result was also verified by Figure 9 (a).

Accordingly, the estimated current density ( $J_{estimated}$ ) is estimated by:

$$J_{estimated} = J_{hopping} + \frac{dE}{dt} \varepsilon_0 \varepsilon_r''(E) \quad (10)$$

As seen in Figure 9 (b), the estimated current density is well coherent with the measured one, suggesting high reliability of the theoretical model depicted in Eq. 10. The fitted loss factor of all 0-3 and 1-3 matrix deduced from Eq. (9) is illustrated in Figure 10, reflecting nonlinear electric field effect of the dielectric loss. Such a nonlinear behavior is consistent to the approach reported on Yang *et al.*, which is deduced from polynomial relationship between the dielectric loss and the applied electric field [22]. The increasing trend of  $\varepsilon_r''$  versus  $E$  shown in Figure 10 is completely different to the model under low electric field, where the dielectric loss is supposed to be stable under a given frequency. The fact is that at high polarization of 1 V/ $\mu\text{m}$ , the conduction mechanism is the dominant contribution, whereas at low polarization of 0.4 V/ $\mu\text{m}$ , the dielectric mechanism is regarded as the primary behavior. Moreover, it was revealed that the simulated dielectric loss factor increases with the increasing ZnO content. Additionally,  $\varepsilon_r''$  is impacted by the distribution of particles due to the increase trend of the free charges and the dipole oscillation in ZnO at low frequency.

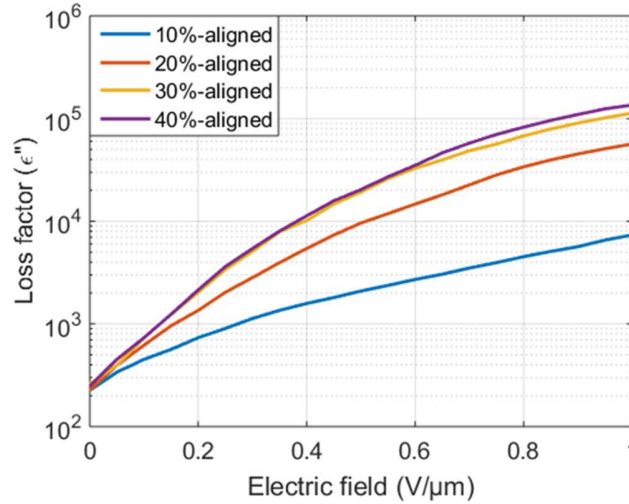


Figure 10. The simulated loss factor derived from the dielectric current for the samples of an aligned structure with different volume fractions.

### 3.6. Mechanical characterization

In this study, mechanical properties are investigated on both 0-3 and 1-3 composites with different particles volume fraction. These materials are subjected to monotonic tensile testing, and their stress-strain

response is displayed in Figure 11 a and b, respectively for the random and aligned samples. A typical stress-strain curve of a polymer as well as its composite consists of 3 phases: 1) a linearity at elastic strain region, 2) a nonlinear behavior in plastic regime, and 3) final fracture [70]. Actually, in most applications of ZnO composites like varistors, energy harvesting, piezoelectric sensor. moderate stress solicitation is usually employed so as not to deteriorate the materials [9,71–73].

Table 4 summarizes the average Young modulus ( $Y$ ) of ZnO/PDMS film obtained through the linear fitting of the initial elastic stress-strain region (Figure 11). A significant enhancement of Young modulus is observed with increasing volume fraction of ZnO, confirming the possibility of tailoring the mechanical properties through the control of the filler content. Indeed, increasing ZnO content makes the film less flexible as more brittle particles added into the matrix. Therefore, the failure strain decreases with ZnO concentration, whereas the failure stress increase. Interestingly, there is no distinct different of Young modulus between the 0-3 and the 1-3 composites. It is probably due to the fact that the dielectrophoretic field direction is not the same as the mechanical tensile testing.

As described in subsection 2.4, it is possible to estimate the ultimate tensile strength ( $T_{max}$ ) of the composites by continuously increasing the applied stress until breakdown occurs (see Figure 11 and Table 4). With the increasing volume fraction, the ultimate tensile strength coherently enhances while the ultimate failure strain decreases, simultaneously. This behavior can be explained due to the defect function of ZnO particles [73].

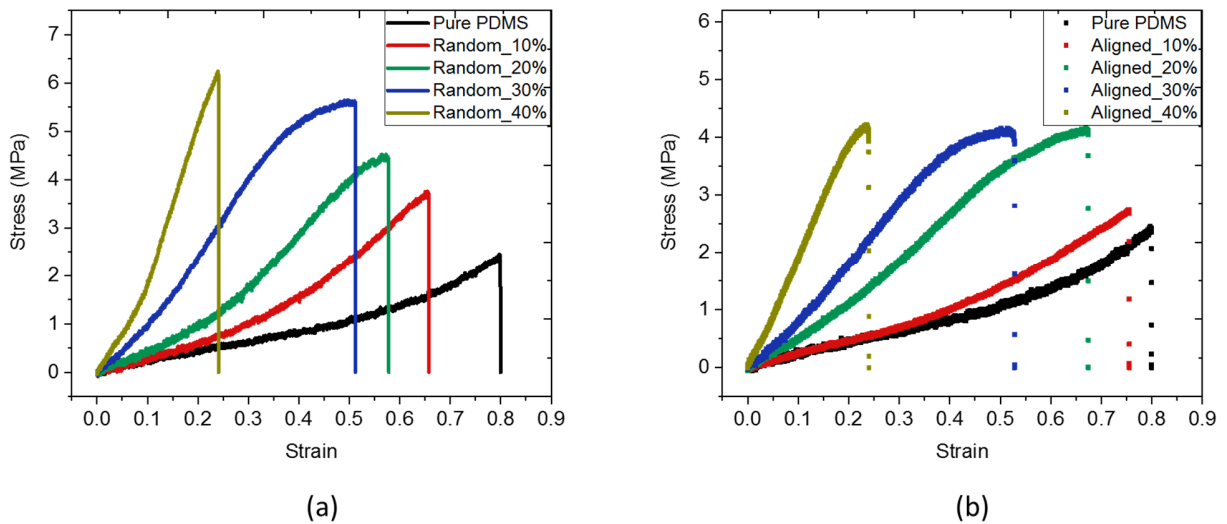


Figure 11. The stress-strain response of (a) random, and (b) aligned-ZnO/PDMS composites with different particle concentrations.

Table 4. The average Young modulus from the fitting data in the linear region

Parameter	Pure PDMS	10% <i>vol</i>	20% <i>vol</i>	30% <i>vol</i>	40% <i>vol</i>
$Y_{random}$ (MPa)	$2.052 \pm 0.002$	$3.254 \pm 0.001$	$6.131 \pm 0.010$	$10.734 \pm 0.015$	$18.256 \pm 0.033$
$Y_{aligned}$ (MPa)	-	$2.076 \pm 0.002$	$6.007 \pm 0.007$	$9.739 \pm 0.008$	$18.593 \pm 0.015$
$T_{max(random)}$ (MPa)	2.435	3.751	4.518	5.628	6.243
$T_{max(aligned)}$ (MPa)	-	2.749	4.166	4.162	4.218

## 4. Potential application of multifunctional ZnO composite for treatment of cardiac arrhythmia

### 4.1. Cardiac arrhythmia treatment based on pulsed field ablation (PFA)

Catheter ablation is a technique employed to treat cardiac arrhythmias that result from abnormal or early activation of myocardium through electrical triggers or aberrant conduction patterns in the myocardium [74]. During the procedure, catheters are delivered percutaneously, typically using femoral venous access and fluoroscopic (X-ray) guidance, to allow placement of catheters at key areas of the heart where the problematic myocardial tissue can be ablated. Usually, the electrodes build above the catheters drive intracardiac electrogram (EGM) voltage signals that are displayed on an electrophysiology recording system [75,76]. These electrograms are used to determine the optimal placement of the ablation catheter for elimination of abnormal electrical signals that initiate the arrhythmia. Local EGMs can be employed as well to evaluate the effectiveness of an ablation, with the goal typically being the annihilation of the local EGM voltage in the tissue targeted for ablation.

Some of the technologies developed over the past three decades for cardiac ablation include radiofrequency (RF) microwave, high intensity focused ultrasound, lasers, and cryogenics. These technologies, however, are often inadequate in eliminating lesion gaps which can lead to recurrence of the arrhythmia and further complicate treatment strategy. Among these, endocardial pulsed field ablation (PFA) is particularly attractive as its non-thermal ablative mechanism shows high benefits to myocardial tissue. This technique creates an instantaneous electrical field to open tiny doors (nano-pores) in nearby cells, a process called “electroporation”. PFA has the potential to completely avoid the collateral injury attendant with all other contemporary thermal energy sources. As reported on the review of F. D. Ramirez *et al.*, cardiomyocytes (heart tissues) have a particularly lower irreversible threshold of electroporation ( $\sim 0.4 \text{ V}/\mu\text{m}$ ) than the other types of cellular like liver ( $\sim 0.6 \text{ V}/\mu\text{m}$ ), kidney ( $\sim 0.7 \text{ V}/\mu\text{m}$ ), vascular smooth muscle cells ( $\sim 1750 \text{ V}/\mu\text{m}$ ), nervous system ( $\sim 3800 \text{ V}/\mu\text{m}$ ) [28]. This makes PFA very tissue selective, which can affect cardiomyocytes while not damaging other surrounding non-heart tissue like nerve fibers or esophagus. Furthermore, unlike the standard ablation energy sources, the PFA catheter does not require actual physical contact but only needs proximity to the tissue to be ablated. As a result, it does not cause scarring or char formation to the patients. In practical terms, this means that PFA is much safer than other current techniques.

The company Farapulse has developed a specific catheter for this procedure, and obtained CE marking since October 2020 [77]. The developed device could generate sufficient electric field in seconds or minutes compared with hours for radiofrequency. The Farapulse generator, which creates the waveform, can be programmed to perform therapy through different catheters. This makes PFA not only very fast but very precise as well. Interestingly, the first functional device of Farapulse paves the way for numerous optimizations in order to enhance the development of such a new method. Also, multifunctional materials are an axis of innovation concerning the development of PFA device. When designing smart catheter based PFA, several issues would be considered, such as 1) the bending angles achievable by the structure; 2) possibility of changing shape from 2D to 3D structure; 3) the degree of rotation needs to be reached and the capacity for miniaturization of the design; and 4) safety of the patients in case of electrical breakdown.

### 4.2. Advantage of using ZnO microvaristor in PFA

The objective of this section reports on the potential of ZnO composite for the development of a smart catheter used in PFA, as described on Figure 12 (a) [78]. The principal scheme of the proposed device is illustrated in Figure 12 (b), where multiple electrodes are deposited above the composite surface. Such a design enables to deliver the PFA energy a series of ultra-short electrical pulses to ablate heart tissue. The overriding constraints of the fabricated materials were related to the following points:

- 1) Mechanical flexibility and biocompatibility;

- 2) electric protection for patient;
- 3) controlling electric field level;
- 4) contact force sensing.

Concerning the first point, it has been demonstrated that PDMS and ZnO are biocompatible properties [79–81], and have the Young modulus and mechanical stiffness compatible with the specification of PFA [82–84]. Moreover, the mechanical properties of the fabricated composites can be somehow adapted by varying the particle concentration.

The second point dedicated to patient safety where electric discharge within heart tissue must be avoided in case of high exceeded electric field application. Actually, ZnO material can be exploited as microvaristor-based over voltage protection, as it can change its resistance value automatically with the change in voltage (cf. Figure 12 (c)). Current commercialized catheters (e.g., Farapulse) used capacitor to build the dielectric layer, which somehow looks similar in size and design to a varistor. However, a simple capacitor cannot suppress voltage surges in the same way a varistor can. When a high voltage surge is accidentally applied to the heart tissue, the outcome would be unimaginable. Therefore, the varistor plays an important role in the protection of patient, and also of electronic circuits from switching spikes and over voltage transients. Under normal operation, the varistor has a very high resistance, allowing lower threshold voltages to pass unaffected. However, when the voltage across the varistor exceeds the percolation value, its effective resistance decreases strongly with an increasing voltage [85]. A typical normalized voltage versus current characteristics curve for a standard varistor is given in Figure 12 (d). Similar result of ZnO composite was previously shown in Figure 3. When not conducting, the I-V curve shows a linear relationship as the current flowing through the varistor remains constant and low at only a few micro-amperes of “leakage” current. This is due to its high resistance acting as an open circuit and remains constant until the voltage across the varistor reaches a particular “switching voltage”. When the transient voltage across the varistor is equal to or greater than that switching value, the resistance of the device suddenly becomes very small, turning the varistor into a conductor due to the avalanche effect of its semiconductor material [86]. In other words, the varistor self-regulates the transient voltage across it by enabling to pass widely varying currents over a narrow voltage range.

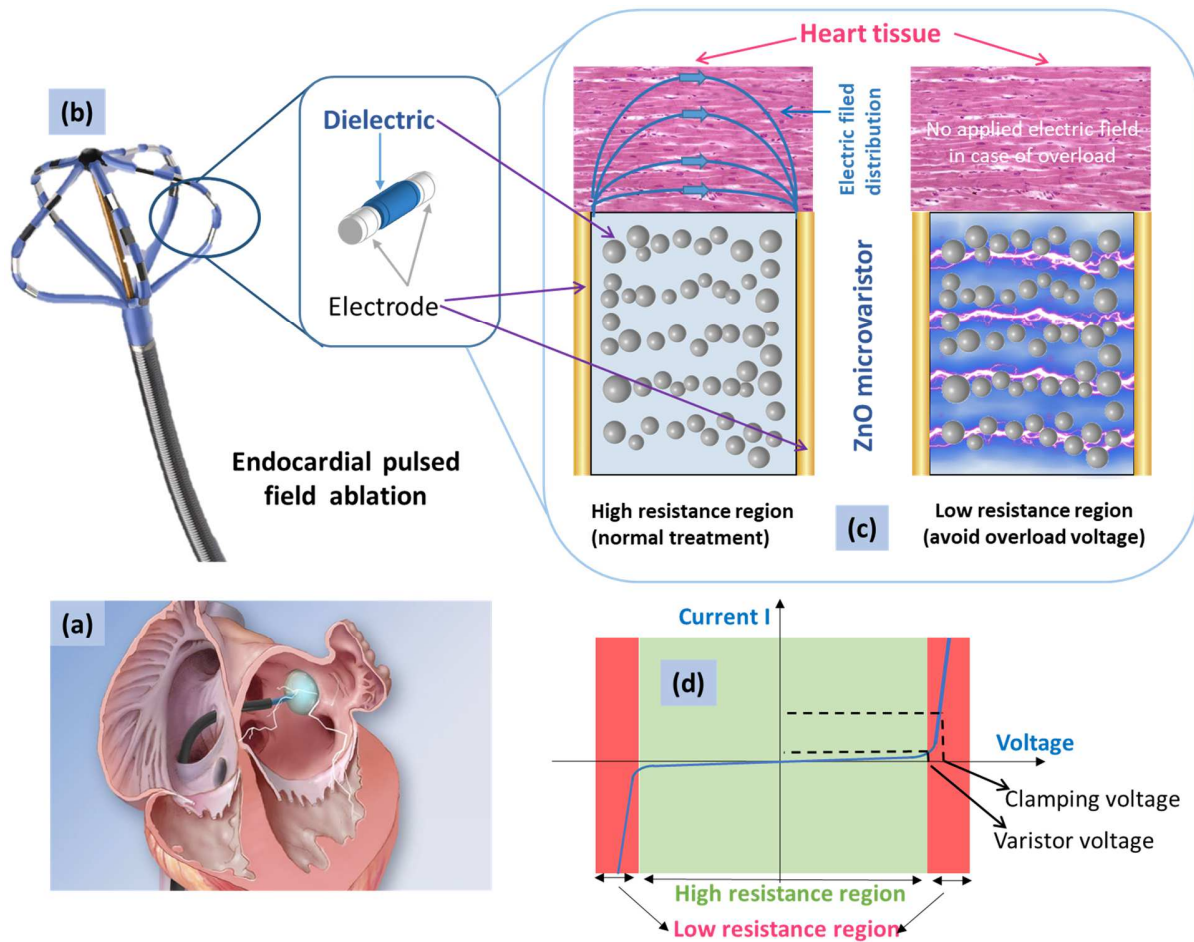


Figure 12. Principle scheme of catheter integrated with ZnO/PDMS microvaristor.

The third issue aims to point out that the electric field subjected to the treated tissue can be simply controlled by varying some relevant parameters. For a better clarification, a simple model consisting of two electrodes sandwiched between the 30% vol. ZnO/PDMS composite and the heart tissue are performed via COMSOL simulation. As seen in Figure 13 (a), one electrode is grounded while the other is subjected to a positive voltage of 10V. Because of large discrepancy in the dielectric permittivity between the PDMS polymer ( $\epsilon_r \sim 2$ ) and the heart tissue ( $\epsilon_r \sim 40$ ) [87], higher electric field level was focused on the polymer matrix. Figure 13 (b) clearly illustrated this behavior, which was in agreement with those found in Pedroli *et al.* [64]. The electric field applied to the heart tissue is situated around  $0.5 \text{ V}/\mu\text{m}$ , i.e. the same order to the irreversible threshold of typically cardiomyocytes. A better adjustment can be carried out to match specified requirement of PFA procedure. Figure 14 depicts evolution of the electric field determined at two specified points. The “point in the middle” locates at the center of the two electrode and around  $5 \mu\text{m}$  up from the bottom of the tissue. The “point at the electrode” situates above the positive electrode, indicating the maximum electric field delivered to the tissue in case of contact. The linear trend between the electric field and the input potential in Figure 14 (a) shows an easy way to get the required electric field level. Figure 14 (b) highlights a significant drop of the electric field with increasing distance between these two electrodes. All results indicated that by playing with different parameters, a desired PFA energy can be successfully obtained.

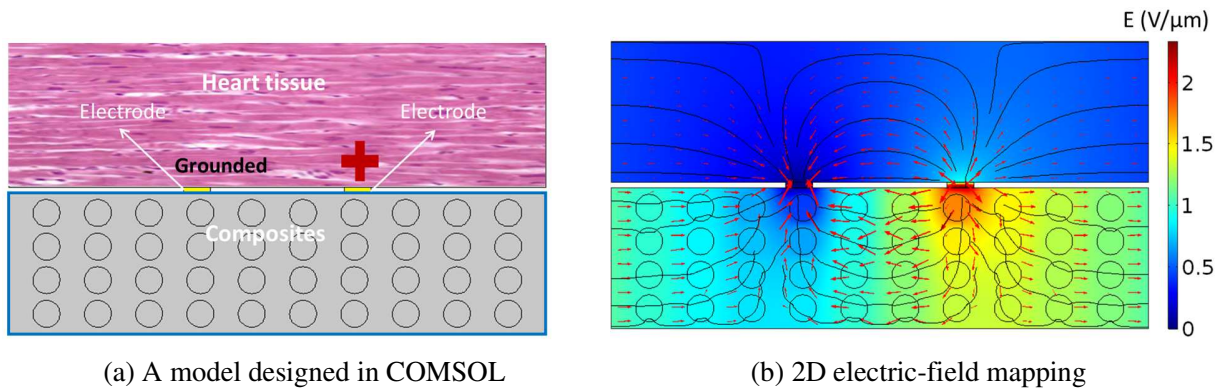


Figure 13. Simulation of ZnO composite and heart tissue subjected to an electric potential of 10 V between two electrodes.

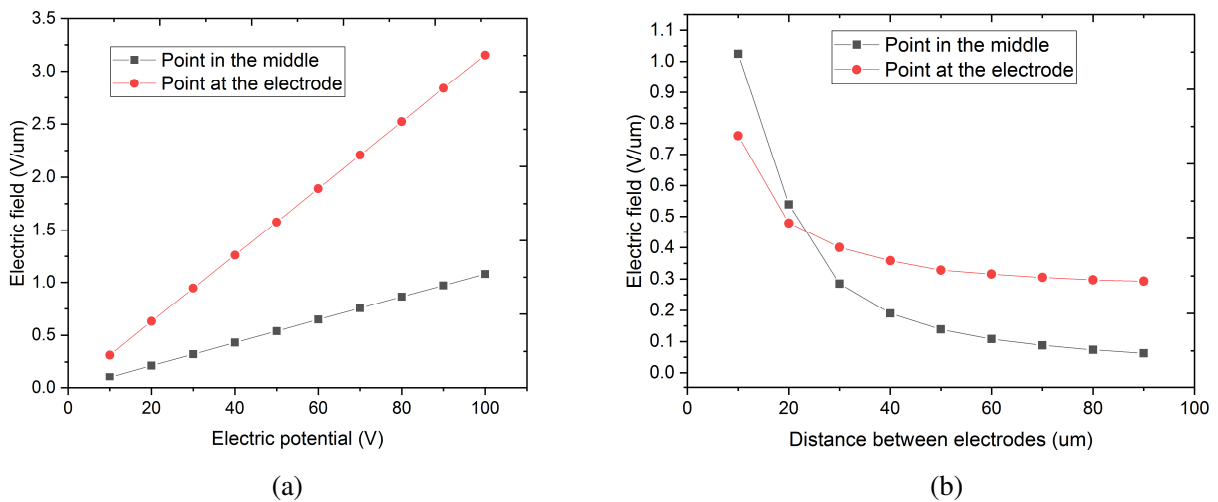


Figure 14. Simulated electric field at 2 specified points as a function of (a) electric potential; and (b) distance between 2 electrodes.

Last but not least, a smart PFA was developed with multifunctionalities, including not only electroporation effect but also sensing ability. One of the key points here involves in performing the contact force (CF) between the ablation electrode and the atrial wall that is a major determinant of lesion size and durability [88]. On one hand, insufficient CF can result in inadequate lesion formation and higher rates of pulmonary vein reconnection [89]. On the other hand, excessive CF leads to complications, such as perforation of tissue. Consequently, monitoring CF would be expected to maximize ablation efficacy and improve safety. Until recent years, CF has been monitored indirectly using a combination of visual observation of catheter tip motion, tactile feedback, local electrogram attenuation, impedance monitoring, and in some laboratories, intracardiac echocardiography. Although widely used, these methods are a poor surrogate for a real-time recording CF. The previous works suggested that ZnO, due to its natural polarity, exhibited piezoelectric effect without requiring polarization process [24]. This makes ZnO as an adequate candidate for force sensor application. Even the piezoelectric sensitivity of ZnO is poor compared to the conventional materials (PZT, BaTiO<sub>3</sub>, PVDF), a simple indicator representing the CF state (e.g. low, medium, high) would be a help to surgeons.

Finally, this study highlighted multifunctional performance of ZnO composite, which depends on various factors like particle concentration, percolation threshold, electric and dielectric properties. External condition like temperature, frequency and amplitude of voltage excitation has an important effect

as well. Optimization of material process through dielectrophoresis is thus of high benefit, which could lead to similar performance by using lower particle concentration and voltage stimulation.

## 5. Conclusion

In this work, a fully characterization of micro-ZnO/PDMS composite was explored to investigate the electrical, dielectric, and mechanical properties. The SEM images indicated a uniform dispersion of micro ZnO particles in the PDMS matrix and showed the formation of aligned particle chains in preferred direction via dielectrophoretic procedure. COMSOL simulation allowed to confirm that the field distribution around the fillers was greatly affected by the material structuration (0-3 vs. 1-3) and the input voltage excitation. In addition, DC nonlinear J-E characteristics indicated that the switch field decreases with increasing filler concentration. Furthermore, dielectrophoretic alignment on the particles clearly enhances the electric response, which is manifested by creation of short conduction paths within the matrix. Also, the temperature dependence of J-E characteristics and dielectric properties were investigated to figure out the working mechanisms. Two factors, namely the carrier transport through ZnO particles and the contact resistance between the fillers, may dominate in different temperature ranges. J-E characteristics test was then performed, clearly illustrating field dependent of two different conduction mechanisms. For the applied field less than  $0.4 \text{ V}/\mu\text{m}$ , capacitive current is regarded as the dominant component and conduction current is linear to the electric field according to the Ohm's law. At  $1 \text{ V}/\mu\text{m}$  which is above the percolation threshold, conduction current turns to be governing and exhibits nonlinear behavior described by the hopping model. Meanwhile, the analysis of bipolar polarization leads to a conclusion of low ferroelectric polarization in ZnO/PDMS composite, reflecting its poor piezoelectric response. Nonetheless, significant improvements in the permittivity and conductivity were achieved for the 1-3 matrix via dielectrophoretic technique. Finally, stress-strain curves were performed using the monotonic uniaxial tensile testing, suggesting an increasing trend of Young modulus of composite with increasing volume fraction of ZnO.

To sum up, ZnO composite with an appropriate switching characteristic, which can be controlled by enhancement of material properties like filler concentration and particle structuration, has shown high potential in microvaristor electronic device. Additionally, the previous work revealed that ZnO material exhibits somewhat piezoelectric response. This property, in addition to excellent nonlinear electric behavior proven by this work, makes ZnO high potential for new design of medical tools; e.g. cardiac catheter ablation where multifunctional modules can be combined. Consequently, general procedures regarding safety requirements, together with biocompatible and sterilizable materials become serious considerations in future works. Another aspect focusses on optimization of material formulation so as to be adaptable to a 3D printer. Such an advancement in fabrication process gives a simple way to achieve miniaturized sensing elements and/or field generator, allowing to facilitate their integration in PFA tools for treatment of cardiac arrhythmia.

## Acknowledgements

This work is supported by ANR (French National Research Agency): ANR-19-CE45-0020-05, ROLLER project, coordinator: Lionel PETIT.

## Declaration of competing interest

The authors have no conflicts of interest to declare.

### **Author's contribution**

XZ, MQL, and PJC wrote and edited the manuscript. XZ and VCN performed experimental tests. XZ plotted data and elaborated composites. MQL provided language help and supervised research. PJC and MQL provided helps on data analysis. JFC gave advice on material fabrications. JFM reviews the manuscript. DG gave idea on medical application. LP validated the feasibility of the project and funds research.

## References

- [1] Ö. Erdem, O.S. Yördem, Y.Z. Mencelo, M. Papila, Poly ( vinylidene fluoride )/ Zinc Oxide Smart Composite Material, 6526 (2007) 1–10. <https://doi.org/10.1117/12.717703>.
- [2] Q. Liu, M.Q. Le, C. Richard, R. Liang, P.J. Cottinet, J.F. Capsal, Enhanced pseudo-piezoelectric dynamic force sensors based on inkjet-printed electrostrictive terpolymer, *Organic Electronics*. 67 (2019) 259–271. <https://doi.org/10.1016/j.orgel.2019.01.028>.
- [3] D. Grinberg, S. Siddique, M.Q. Le, R. Liang, J.F. Capsal, P.J. Cottinet, 4D Printing based piezoelectric composite for medical applications, *Journal of Polymer Science, Part B: Polymer Physics*. 57 (2019) 109–115. <https://doi.org/10.1002/polb.24763>.
- [4] M.Q. Le, J.F. Capsal, J. Galineau, F. Ganet, X. Yin, M.D. Yang, J.F. Chateaux, L. Renaud, C. Malhaire, P.J. Cottinet, R. Liang, All-organic electrostrictive polymer composites with low driving electrical voltages for micro-fluidic pump applications, *Scientific Reports*. 5 (2015) 1–13. <https://doi.org/10.1038/srep11814>.
- [5] F. Ganet, M.Q. Le, J.F. Capsal, J.F. Gérard, S. Pruvost, J. Duchet-Rumeau, S. Livi, P. Lermusiaux, A. Millon, P.J. Cottinet, Haptic feedback using an all-organic electroactive polymer composite, *Sensors and Actuators, B: Chemical*. 220 (2015) 1120–1130. <https://doi.org/10.1016/j.snb.2015.06.071>.
- [6] A.S. Roy, S. Gupta, S. Sindhu, A. Parveen, P.C. Ramamurthy, Dielectric properties of novel PVA/ZnO hybrid nanocomposite films, *Composites Part B: Engineering*. 47 (2013) 314–319. <https://doi.org/10.1016/j.compositesb.2012.10.029>.
- [7] S. Ishibe, M. Mori, M. Kozako, A New Concept Varistor With Epoxy / Microvaristor Composite, 29 (2014) 677–682.
- [8] N. Bouropoulos, G.C. Psarras, N. Moustakas, A. Chrissanthopoulos, S. Baskoutas, Optical and dielectric properties of ZnO-PVA nanocomposites, *Physica Status Solidi (a)*. 205 (2008) 2033–2037. <https://doi.org/10.1002/pssa.200778863>.
- [9] K.J. Loh, D. Chang, Zinc oxide nanoparticle-polymeric thin films for dynamic strain sensing, *Journal of Materials Science*. 46 (2011) 228–237. <https://doi.org/10.1007/s10853-010-4940-3>.
- [10] J.S. Dodds, F.N. Meyers, K.J. Loh, Piezoelectric nanocomposite sensors assembled using zinc oxide nanoparticles and poly(vinylidene fluoride), *Smart Structures and Systems*. 12 (2013) 55–71. <https://doi.org/10.12989/sss.2013.12.1.055>.
- [11] Z. Meng, H. Zhang, M. Zhu, X. Wei, J. Cao, I. Murtaza, M.U. Ali, H. Meng, J. Xu, Lead Zirconate Titanate (a piezoelectric ceramic)-Based thermal and tactile bimodal organic transistor sensors, *Organic Electronics*. 80 (2020) 105673. <https://doi.org/10.1016/j.orgel.2020.105673>.
- [12] S. Yan, C. Sun, Q. Cui, M. He, Willhandy, R. Wang, J. Hao, X. Chu, Dielectric, piezoelectric and dc bias characteristics of Bi-doped PZT multilayer ceramic actuator, *Materials Chemistry and Physics*. 255 (2020) 123605. <https://doi.org/10.1016/j.matchemphys.2020.123605>.
- [13] G. D’Ambrogio, O. Zahhaf, Y. Hebrard, M.Q. Le, P. Cottinet, J. Capsal, Micro-Structuration of Piezoelectric Composites Using Dielectrophoresis: Toward Application in Condition Monitoring of Bearings, *Advanced Engineering Materials*. (2020) 2000773. <https://doi.org/10.1002/adem.202000773>.
- [14] M. Kandpal, C. Sharan, P. Poddar, K. Prashanthi, P.R. Apte, V. Ramgopal Rao, Photopatternable nanocomposite (SU-8/ZnO) thin films for piezo-electric applications, *Applied Physics Letters*. 101 (2012). <https://doi.org/10.1063/1.4748575>.
- [15] T. Chen, M.-H. Wang, H.-P. Zhang, Z.-Y. Zhao, T.-T. Liu, Novel synthesis of monodisperse ZnO-based core/shell ceramic powders and applications in low-voltage varistors, *Materials & Design*. 96 (2016) 329–334. <https://doi.org/10.1016/j.matdes.2016.02.015>.
- [16] L. Donzel, F. Greuter, T. Christen, Nonlinear resistive electric field grading part 2: Materials and applications, *IEEE Electrical Insulation Magazine*. 27 (2011) 18–29. <https://doi.org/10.1109/MEI.2011.5739419>.

- [17] D. Weida, C. Richter, M. Clemens, Design of ZnO microvaristor material stress-cone for cable accessories, *IEEE Transactions on Dielectrics and Electrical Insulation*. 18 (2011) 1262–1267. <https://doi.org/10.1109/TDEI.2011.5976125>.
- [18] K.P. Donnelly, B.R. Varlow, Non-linear dc and ac conductivity in electrically insulating composites, *IEEE Transactions on Dielectrics and Electrical Insulation*. 10 (2003) 610–614. <https://doi.org/10.1109/TDEI.2003.1219645>.
- [19] C.C. Lin, W.S. Lee, C.C. Sun, W.H. Whu, A varistor-polymer composite with nonlinear electrical-thermal switching properties, *Ceramics International*. 34 (2008) 131–136. <https://doi.org/10.1016/j.ceramint.2006.09.018>.
- [20] F. Chiu, A Review on Conduction Mechanisms in Dielectric Films, 2014 (2014).
- [21] F.C. Chiu, C.Y. Lee, T.M. Pan, Current conduction mechanisms in Pr<sub>2</sub>O<sub>3</sub>/oxynitride laminated gate dielectrics, *Journal of Applied Physics*. 105 (2009) 074103. <https://doi.org/10.1063/1.3103282>.
- [22] Z. Yang, J. Zu, Comparison of PZN-PT, PMN-PT single crystals and PZT ceramic for vibration energy harvesting, *Energy Conversion and Management*. 122 (2016) 321–329. <https://doi.org/10.1016/j.enconman.2016.05.085>.
- [23] D.W. Auckland, N.E. Brown, B.R. Varlow, Non-linear conductivity in electrical insulation, in: *Conference on Electrical Insulation and Dielectric Phenomena (CEIDP), Annual Report, IEEE, 1997*: pp. 186–189. <https://doi.org/10.1109/ceidp.1997.634590>.
- [24] X. Zhang, M.Q. Le, O. Zahhaf, J.F. Capsal, P.J. Cottinet, L. Petit, Enhancing dielectric and piezoelectric properties of micro-ZnO/PDMS composite-based dielectrophoresis, *Materials and Design*. 192 (2020) 108783. <https://doi.org/10.1016/j.matdes.2020.108783>.
- [25] K. (Ed.) Uchino, *Advanced piezoelectric materials: Science and technology*, Woodhead Publishing, 2017.
- [26] R.E. Newnham, D.P. Skinner, L.E. Cross, Connectivity and piezoelectric-pyroelectric composites, *Materials Research Bulletin*. 13 (1978) 525–536. [https://doi.org/10.1016/0025-5408\(78\)90161-7](https://doi.org/10.1016/0025-5408(78)90161-7).
- [27] I. Babu, G. de With, Highly flexible piezoelectric 0-3 PZT-PDMS composites with high filler content, *Composites Science and Technology*. 91 (2014) 91–97. <https://doi.org/10.1016/j.compscitech.2013.11.027>.
- [28] F.D. Ramirez, V.Y. Reddy, R. Viswanathan, M. Hocini, P. Jaïs, Emerging Technologies for Pulmonary Vein Isolation, *Circulation Research*. 127 (2020) 170–183. <https://doi.org/10.1161/CIRCRESAHA.120.316402>.
- [29] K. Goc, K. Gaska, K. Klimczyk, A. Wujek, W. Prendota, L. Jarosinski, A. Rybak, G. Kmita, C. Kapusta, Influence of magnetic field-aided filler orientation on structure and transport properties of ferrite filled composites, *Journal of Magnetism and Magnetic Materials*. 419 (2016) 345–353. <https://doi.org/10.1016/j.jmmm.2016.06.046>.
- [30] C.Y. Liu, A.J. Bard, Pressure-induced insulator-conductor transition in a photoconducting organic liquid-crystal film, *Nature*. 418 (2002) 162–164. <https://doi.org/10.1038/nature00875>.
- [31] H. Ahmad, A. Haddad, H. Griffiths, S. Robson, T. Nishimura, N. Tsukamoto, Electrical characterisation of ZnO microvaristor materials and compounds, in: *Annual Report - Conference on Electrical Insulation and Dielectric Phenomena, CEIDP, Institute of Electrical and Electronics Engineers Inc., 2015*: pp. 688–692. <https://doi.org/10.1109/CEIDP.2015.7352035>.
- [32] A.K. Jonscher, Physical basis of dielectric loss, *Nature*. 253 (1975) 717–719. <https://doi.org/10.1038/253717a0>.
- [33] Ashim Kumar Bain, Prem Chand, *Dielectric Properties of Materials*, in: *Ferroelectrics*, John Wiley & Sons, Ltd, 2017: pp. 1–18. <https://doi.org/10.1002/9783527805310.ch1>.
- [34] F. Pedroli, A. Flocchini, A. Marrani, M.-Q. Le, O. Sanseau, P.-J. Cottinet, J.-F. Capsal, Boosted energy-storage efficiency by controlling conduction loss of multilayered polymeric capacitors, *Materials & Design*. 192 (2020) 108712. <https://doi.org/10.1016/j.matdes.2020.108712>.

- [35] X. Yang, X. Zhao, H. Jinliang, Grading Electric Field in High Voltage Insulation Using Composite Materials, (2018). <https://doi.org/10.1109/MEI.2018.8246118>.
- [36] X. Yang, J. Hu, S. Chen, J. He, Understanding the Percolation Characteristics of Nonlinear Composite Dielectrics, *Scientific Reports*. 6 (2016) 1–11. <https://doi.org/10.1038/srep30597>.
- [37] K. Eda, Zinc Oxide Varistors, *IEEE Electrical Insulation Magazine*. 5 (1989) 28–30. <https://doi.org/10.1109/57.44606>.
- [38] M.M. Saadeldin, O.A. Desouky, M. Ibrahim, G.E. Khalil, Investigation of structural and electrical properties of ZnO varistor samples doped with different additives, *NRIAG Journal of Astronomy and Geophysics*. 7 (2019) 201–207. <https://doi.org/10.1016/j.nrjag.2018.06.002>.
- [39] N. Yamamoto, H. Makino, T. Yamamoto, Young's modulus and coefficient of linear thermal expansion of ZnO conductive and transparent ultra-thin films, *Advances in Materials Science and Engineering*. 2011 (2011). <https://doi.org/10.1155/2011/136127>.
- [40] B.E. Schubert, Electronic Supplementary Information (ESI): Variable stiffness material based on rigid low-melting-point-alloy-microstructures embedded in soft poly ( dimethylsiloxane ) ( PDMS ), (2013) 3–5.
- [41] R. Strümpfer, J. Glatz-Reichenbach, Conducting polymer composites, *Journal of Electroceramics*. 3 (1999) 329–346. <https://doi.org/10.1023/A:1009909812823>.
- [42] Y.P. Varshni, Temperature dependence of the energy gap in semiconductors, *Physica*. 34 (1967) 149–154. [https://doi.org/10.1016/0031-8914\(67\)90062-6](https://doi.org/10.1016/0031-8914(67)90062-6).
- [43] F.H. Abd El-kader, S.A. Gaafer, K.H. Mahmoud, S.I. Mohamed, M.F.H. Abd El-kader, Electrical conduction in (polyvinyl alcohol/glycogen) blend films, *Polymer Composites*. 30 (2009) 214–220. <https://doi.org/10.1002/pc.20553>.
- [44] J.F. Capsal, M. Lallart, J. Galineau, P.J. Cottinet, G. Sebald, D. Guyomar, Evaluation of macroscopic polarization and actuation abilities of electrostrictive dipolar polymers using the microscopic Debye/Langevin formalism, *Journal of Physics D: Applied Physics*. 45 (2012). <https://doi.org/10.1088/0022-3727/45/20/205401>.
- [45] N. Della Schiava, M.-Q. Le, J. Galineau, F. Domingues Dos Santos, P.-J. Cottinet, J.-F. Capsal, Influence of Plasticizers on the Electromechanical Behavior of a P(VDF-TrFE-CTFE) Terpolymer: Toward a High Performance of Electrostrictive Blends, *Journal of Polymer Science Part B: Polymer Physics*. 55 (2017) 355–369. <https://doi.org/10.1002/polb.24280>.
- [46] M. Akram, A. Javed, T.Z. Rizvi, Dielectric properties of industrial polymer composite materials, *Turkish Journal of Physics*. 29 (2005) 355–362. <https://doi.org/10.22401/jnus.13.1.10>.
- [47] W.A. Hussain, A.A. Hussein, J.M. Khalaf, A.H. Al-Mowali, A.A. Sultan, Dielectric Properties and a.c. Conductivity of Epoxy/Alumina Silicate NGK Composites, *Advances in Chemical Engineering and Science*. 05 (2015) 282–289. <https://doi.org/10.4236/aces.2015.53028>.
- [48] F. Pedroli, A. Marrani, M.-Q. Le, O. Sanseau, P.-J. Cottinet, J.-F. Capsal, Reducing leakage current and dielectric losses of electroactive polymers through electro-annealing for high-voltage actuation, *RSC Adv*. 9 (2019) 12823–12835. <https://doi.org/10.1039/C9RA01469A>.
- [49] Das, Sourav, Synthesis, characterization and dielectric properties of nanocrystalline nickel, *Indian Journal of Pure & Applied Physics (IJPAP)*. 52 (2015) 386–390.
- [50] B.A. Aldar, R.K. Pinjari, N.M. Burange, Electric and Dielectric behavior of Ni-Co-Cd Ferrite, n.d.
- [51] J.R. Macdonald, Theory of ac space-charge polarization effects in photoconductors, semiconductors, and electrolytes, *Physical Review*. 92 (1953) 4–17. <https://doi.org/10.1103/PhysRev.92.4>.
- [52] J.-F. Capsal, M. Lallart, J. Galineau, P.-J. Cottinet, G. Sebald, D. Guyomar, Evaluation of macroscopic polarization and actuation abilities of electrostrictive dipolar polymers using the microscopic Debye/Langevin formalism, *J. Phys. D: Appl. Phys.* 45 (2012) 205401. <https://doi.org/10.1088/0022-3727/45/20/205401>.

- [53] C. Zhang, D. Wang, J. He, M. Liu, G.-H. Hu, Z.-M. Dang, Synthesis, nanostructures and dielectric properties of novel liquid crystalline block copolymers, *Polym. Chem.* 5 (2014) 2513–2520. <https://doi.org/10.1039/C3PY01522J>.
- [54] G.L. Wang, Y.Y. Zhang, J. Zhang, K.H. Ding, Z.F. Wang, M. Zhang, Preparation and electrodeformation of silicone dielectric elastomers containing poly(propylene glycol diacetate) with different molecular weights, *Journal of Applied Polymer Science.* 134 (2017) 45329. <https://doi.org/10.1002/app.45329>.
- [55] X. Huang, H. Zhang, Y. Lai, J. Li, The lowered dielectric loss tangent and grain boundary effects in fluorine-doped calcium copper titanate ceramics, *Appl. Phys. A.* 123 (2017) 317. <https://doi.org/10.1007/s00339-017-0947-9>.
- [56] L. Ramajo, M. Reboredo, M. Castro, Dielectric response and relaxation phenomena in composites of epoxy resin with BaTiO<sub>3</sub> particles, *Composites Part A: Applied Science and Manufacturing.* 36 (2005) 1267–1274. <https://doi.org/10.1016/j.compositesa.2005.01.026>.
- [57] N. Hadik, A. Outzourhit, A. Elmansouri, A. Abouelaoualim, A. Oueriagli, E.L. Ameziane, Dielectric behavior of ceramic (BST)/epoxy thick films, *Active and Passive Electronic Components.* 2009 (2009) 1–7. <https://doi.org/10.1155/2009/437130>.
- [58] M.K. Gupta, N. Sinha, B.K. Singh, N. Singh, K. Kumar, B. Kumar, Piezoelectric, dielectric, optical and electrical characterization of solution grown flower-like ZnO nanocrystal, *Materials Letters.* 63 (2009) 1910–1913. <https://doi.org/10.1016/j.matlet.2009.06.003>.
- [59] S. Bhattacharyya, S.K. Saha, D. Chakravorty, Nanowire formation in a polymeric film, *Applied Physics Letters.* 76 (2000) 3896–3898. <https://doi.org/10.1063/1.126813>.
- [60] J. Belovickis, J. Macutkevicius, Š. Svirskas, V. Samulionis, J. Banys, Ferroelectrics Dielectric Spectroscopy of Polymer Based PDMS Nanocomposites with ZnO Nanoparticles, (2015) 37–41. <https://doi.org/10.1080/00150193.2015.1012016>.
- [61] J.S. Dodds, F.N. Meyers, K.J. Loh, Piezoelectric characterization of PVDF-TrFE thin films enhanced with ZnO nanoparticles, *IEEE Sensors Journal.* 12 (2012) 1889–1890. <https://doi.org/10.1109/JSEN.2011.2182043>.
- [62] A. Morel, G. Pillonnet, Y. Wanderoild, A. Badel, Dielectric losses considerations for piezoelectric energy harvesting, *Journal of Low Power Electronics.* 14 (2018) 244–254. <https://doi.org/10.1166/jolpe.2018.1562>.
- [63] G. Liu, S. Zhang, W. Jiang, W. Cao, Losses in ferroelectric materials, *Materials Science and Engineering: R: Reports.* 89 (2015) 1–48. <https://doi.org/10.1016/j.mser.2015.01.002>.
- [64] F. Pedroli, A. Marrani, M.-Q. Le, C. Froidefond, P.-J. Cottinet, J.-F. Capsal, Processing optimization: A way to improve the ionic conductivity and dielectric loss of electroactive polymers, *Journal of Polymer Science Part B: Polymer Physics.* 56 (2018) 1164–1173. <https://doi.org/10.1002/polb.24636>.
- [65] A. Chaipanich, Dielectric and piezoelectric properties of PZT-cement composites, *Current Applied Physics.* 7 (2007) 537–539. <https://doi.org/10.1016/j.cap.2006.10.015>.
- [66] R. Li, Z. Zhao, Z. Chen, J. Pei, Novel BaTiO<sub>3</sub>/PVDF composites with enhanced electrical properties modified by calcined BaTiO<sub>3</sub> ceramic powders, *Materials Express.* 7 (2017) 536–540. <https://doi.org/10.1166/mex.2017.1393>.
- [67] A.M. Nardes, M. Kemerink, R.A.J. Janssen, Anisotropic hopping conduction in spin-coated PEDOT:PSS thin films, *Physical Review B - Condensed Matter and Materials Physics.* 76 (2007) 085208. <https://doi.org/10.1103/PhysRevB.76.085208>.
- [68] I. Glowacki, J. Jung, J. Ulanski, A. Rybak, Conductivity Measurements, in: *Polymer Science: A Comprehensive Reference*, 10 Volume Set, Elsevier, 2012: pp. 847–877. <https://doi.org/10.1016/B978-0-444-53349-4.00058-3>.
- [69] T. Miyamoto, K. Shibayama, Free-volume model for ionic conductivity in polymers, *Journal of Applied Physics.* 44 (1973) 5372–5376. <https://doi.org/10.1063/1.1662158>.

- [70] C. Miehe, S. Göktepe, J. Méndez Diez, Finite viscoplasticity of amorphous glassy polymers in the logarithmic strain space, *International Journal of Solids and Structures*. 46 (2009) 181–202. <https://doi.org/10.1016/j.ijsolstr.2008.08.029>.
- [71] Z.L. Wang, ZnO nanowire and nanobelt platform for nanotechnology, *Materials Science and Engineering: R: Reports*. 64 (2009) 33–71. <https://doi.org/10.1016/J.MSER.2009.02.001>.
- [72] R. Hinchet, J. Ferreira, J. Keraudy, G. Ardila, E. Pauliac-Vaujour, M. Mouis, L. Montes, Scaling rules of piezoelectric nanowires in view of sensor and energy harvester integration, *Technical Digest - International Electron Devices Meeting, IEDM*. (2012) 119–122. <https://doi.org/10.1109/IEDM.2012.6478988>.
- [73] J. He, Introduction of Varistor Ceramics, *Metal Oxide Varistors*. (2019) 1–30. <https://doi.org/10.1002/9783527684038.ch1>.
- [74] P. Kramar, D. Miklavčič, L.M. Mir, Electroporation-based Technologies and Treatments Proceedings of the Electroporation-based Technologies and Treatments International SCIENTIFIC WORKSHOP and POSTGRADUATE COURSE, n.d.
- [75] R. Gopinathannair, F.M. Merchant, D.R. Lakkireddy, S.P. Etheridge, S. Feigofsky, J.K. Han, R. Kabra, A. Natale, S. Poe, S.A. Saha, A.M. Russo, COVID-19 and cardiac arrhythmias: a global perspective on arrhythmia characteristics and management strategies, *J Interv Card Electrophysiol*. (2020) 1–8. <https://doi.org/10.1007/s10840-020-00789-9>.
- [76] Stavrakis Stavros, Kulkarni Kanchan, Singh Jagmeet P., Katritsis Demosthenes G., Armoundas Antonis A., Autonomic Modulation of Cardiac Arrhythmias, *JACC: Clinical Electrophysiology*. 6 (2020) 467–483. <https://doi.org/10.1016/j.jacep.2020.02.014>.
- [77] V.Y. Reddy, P. Neuzil, J.S. Koruth, J. Petru, M. Funosako, H. Cochet, L. Sediva, M. Chovanec, S.R. Dukkipati, P. Jais, Pulsed Field Ablation for Pulmonary Vein Isolation in Atrial Fibrillation, *Journal of the American College of Cardiology*. 74 (2019) 315–326. <https://doi.org/10.1016/j.jacc.2019.04.021>.
- [78] V.Y. Reddy, A. Anic, J. Koruth, J. Petru, M. Funasako, K. Minami, T. Breskovic, I. Sikiric, S.R. Dukkipati, I. Kawamura, P. Neuzil, Pulsed Field Ablation in Patients With Persistent Atrial Fibrillation, *Journal of the American College of Cardiology*. 76 (2020) 1068–1080. <https://doi.org/10.1016/j.jacc.2020.07.007>.
- [79] X. Jing, Z. Guo, Fabrication of biocompatible super stable lubricant-immobilized slippery surfaces by grafting a polydimethylsiloxane brush: Excellent boiling water resistance, hot liquid repellency and long-term slippery stability, *Nanoscale*. 11 (2019) 8870–8881. <https://doi.org/10.1039/c9nr01556f>.
- [80] Y. Chen, W.H. Tse, L. Chen, J. Zhang, Ag nanoparticles-decorated ZnO nanorod array on a mechanical flexible substrate with enhanced optical and antimicrobial properties, *Nanoscale Research Letters*. 10 (2015) 106. <https://doi.org/10.1186/s11671-014-0712-3>.
- [81] S. Jakmuangpak, T. Prada, W. Mongkolthananaruk, V. Harnchana, S. Pinitsoontorn, Engineering Bacterial Cellulose Films by Nanocomposite Approach and Surface Modification for Biocompatible Triboelectric Nanogenerator, *ACS Applied Electronic Materials*. 2 (2020) 2498–2506. <https://doi.org/10.1021/acsaelm.0c00421>.
- [82] Y. Ateş, C.A. Yücesoy, M.A. Ünlü, B. Saygin, N. Akkaş, The Mechanical Properties of Intact and Traumatized Epidural Catheters, *Anesthesia & Analgesia*. 90 (2000) 393. <https://doi.org/10.1213/00000539-200002000-00029>.
- [83] L. Blanc, A. Delchambre, P. Lambert, Flexible medical devices: Review of controllable stiffness solutions, *Actuators*. 6 (2017). <https://doi.org/10.3390/act6030023>.
- [84] Y. Shirasaki, K. Yoshizawa, T. Tateishi, Changes in the mechanical properties of silicone catheter in degrading process, *Nihon Reorogi Gakkaishi*. 29 (2001) 9–13. <https://doi.org/10.1678/rheology.29.9>.
- [85] E. Olsson, L.K.L. Falk, G.L. Dunlop, R. Österlund, The microstructure of a ZnO varistor material, *J Mater Sci*. 20 (1985) 4091–4098. <https://doi.org/10.1007/BF00552403>.

- [86] S.C. Pillai, J.M. Kelly, R. Ramesh, D.E. McCormack, Advances in the synthesis of ZnO nanomaterials for varistor devices, *J. Mater. Chem. C*. 1 (2013) 3268–3281. <https://doi.org/10.1039/C3TC00575E>.
- [87] M. Schaefer, W. Gross, J. Ackemann, M.M. Gebhard, The complex dielectric spectrum of heart tissue during ischemia, *Bioelectrochemistry*. 58 (2002) 171–180. [https://doi.org/10.1016/S1567-5394\(02\)00152-4](https://doi.org/10.1016/S1567-5394(02)00152-4).
- [88] A.S. Barnett, T.D. Bahnson, J.P. Piccini, Recent Advances in Lesion Formation for Catheter Ablation of Atrial Fibrillation, *Circulation: Arrhythmia and Electrophysiology*. 9 (2016). <https://doi.org/10.1161/CIRCEP.115.003299>.
- [89] A. Aryana, S.M. Singh, G. Mugnai, C. de Asmundis, M. Kowalski, D.K. Pujara, A.I. Cohen, S.K. Singh, C.E. Fuenzalida, N. Prager, M.R. Bowers, P.G. O'Neill, P. Brugada, A. d'Avila, G.B. Chierchia, Pulmonary vein reconnection following catheter ablation of atrial fibrillation using the second-generation cryoballoon versus open-irrigated radiofrequency: results of a multicenter analysis, *Journal of Interventional Cardiac Electrophysiology*. 47 (2016) 341–348. <https://doi.org/10.1007/s10840-016-0172-z>.

